Impact of Intermediate Nanomachines in Multiple Cooperative Nanomachine-Assisted Diffusion Advection Mobile Molecular Communication

Neeraj Varshney, *Student Member, IEEE*, Adarsh Patel, *Member, IEEE*, Werner Haselmayr, *Member, IEEE*, Aditya K. Jagannatham, *Member, IEEE*, Pramod K. Varshney, *Life Fellow, IEEE*, and Arumugam Nallanathan, *Fellow, IEEE*

***Abstract*—Motivated by the numerous healthcare applications of molecular communication inside blood vessels of the human body, this work considers multiple relay/ cooperative nanomachine (CN)-assisted molecular communication between a source nanomachine (SN) and a destination nanomachine (DN) where each nanomachine is mobile in a diffusion-advection flow channel. Using the first hitting time model, the impact of the intermediate CNs on the performance of the aforementioned system with fully absorbing receivers is comprehensively analyzed taking into account the presence of various degrading factors such as inter-symbol interference, multi-source interference, and counting errors. For this purpose, the optimal decision rules are derived for symbol detection at each of the CNs as well as the DN. Further, closed-form expressions are derived for the probabilities of detection and false alarm at each CN and DN, along with the overall end-to-end probability of error and channel achievable rate for communication between the SN and DN. Simulation results are presented to corroborate the theoretical results derived and also, to yield insights into the system performance under various mobility conditions.**

***Index Terms*—Cooperative nanomachines, diffusion, fully absorbing receivers, Likelihood Ratio Test (LRT), mobile molecular communication, optimal detection.**

I. Introduction

NANOSCALE molecular communication (MC), where the information exchange is done using chemical signals, has garnered significant interest in recent times towards addressing challenging problems in biomedical, industrial, and surveillance applications [2], [3]. Currently, MC research can be categorized into three major areas: 1) Living system modelling, which is aimed at gaining more insights into MC processes occurring in live biological systems leveraging techniques originating from communications engineering. For example, in [4], information theoretic concepts were used to quantify the information exchange in protein structures. 2) Living system interface, which targets controlling the behavior of biological systems. As an example, in the work in [5], the redox modality has been used to connect synthetic biology to electronics for bio-device communication. 3) Artificial MC that is aimed at the design, fabrication and testing of human-made MC systems, which forms the focus of this work. A salient example of such research is the inexpensive experimental platform that was presented in [6], which can be used to simulate MC in different environments, such as in cardiovascular systems and others. Moreover, a paradigm for chemical communication between gated nanoparticles was recently demonstrated in [7].

A. Motivation

Artificial MC has led to the development of novel applications [8]–[10] such as efficient chrono drug-delivery [11] and human body monitoring using communicating nano-robots or nanomachines, which has been used for detection and monitoring of cholesterol or disease precursors in blood vessels [12]. To realize an efficient chrono drug-delivery mechanism, a nanomachine in one part of the body can sense an event and communicate this information to a drug-delivery nanomachine in another part of the body using molecular signaling via the circulation system with advection flow [11]. However, in such scenarios, the molecular concentration decays inversely as the cube of the distance between the mobile transmitter and mobile receiver nanomachines [13], which severely limits the performance of such systems. This impediment can be successfully overcome by relay or cooperative nanomachine (CN)-assisted communication, where one or multiple mobile CNs cooperate with a mobile source nanomachine (SN) in forwarding information to a mobile destination nanomachine (DN). This paradigm has been shown to significantly enhance the communication range, thus making it a very promising technology for such systems [14]. However, the decoding accuracy at the DN in a multiple CN-assisted MC system relies considerably on the detection performance of the intermediate CNs that act as relays. The end-to-end performance can further deteriorate due to other degrading effects such as mobility, inter-symbol interference (ISI), multi-source interference (MSI), and counting errors at the intermediate CNs as well as at the DN [15]. This motivates us to analyze the impact of the detection performance of the intermediate mobile CNs on the end-to-end performance of the multiple CN-assisted MC system, along with the presence of ISI, MSI, and counting errors, for a diffusion-advection blood flow channel. A detailed

The part of this paper considering the presence of a single cooperative nanomachine (CN) has been presented at the 2018 Asilomar Conference on Signals, Systems, and Computers [1].

Neeraj Varshney and Aditya K. Jagannatham are with the Department of Electrical Engineering, Indian Institute of Technology Kanpur, UP, India (e-mail:{neerajv; adityaj}@iitk.ac.in).

Adarsh Patel and Pramod K. Varshney are with the Department of Electrical Engineering & Computer Science, Syracuse University, Syracuse, New York, USA (e-mail:{apatel31; varshney}@syr.edu).

Werner Haselmayr is with the Johannes Kepler University Linz, Austria (email: werner.haselmayr@jku.at).

Arumugam Nallanathan is with the Queen Mary University of London, London, United Kingdom (email: nallanathan@ieee.org).

overview and a comparative survey of related works in the literature on CN-assisted MC is presented next.

B. Related Work and Contributions

In [16], a sense-and-forward (SF) relaying strategy has been proposed for diffusive MC between two synthetic bacteria nodes. The analysis therein has been extended in [17] to MC with decode-and-forward (DF) relaying where it was demonstrated that optimal combining of the direct and relayed outputs led to an improvement in the reliability of communication. Authors in [18] derived an expression to characterize the average probability of error for a two-hop DF molecular network and subsequently proposed techniques to mitigate the self-interference arising due to the reception and emission of the same type of molecules at the relay. The analysis has been further extended to amplify-and-forward (AF) relaying-based MC with fixed and variable amplification factors in [19]. The optimal amplification factor at the relay node that minimizes the approximate average error probability of the network is also derived therein. The authors in [20], [21] proposed an energy efficient scheme for information molecule synthesis employing simultaneous molecular information and energy transfer (SMIET) relaying. Performance analysis was presented in [21] for the resulting bit error probability and cost of synthesis. In [22], the performance of a dual-hop MC system with estimate-and-forward (EF) relaying has been analyzed in terms of the resulting molecular throughput and probability of error considering the effect of residual and counting noises. The work in [23] analyzed the error rate performance of a diffusion-based DF dual-hop MC system inside a blood vessel of the human body, assuming pure diffusion based MC with static nanomachines, which is not practically feasible in diffusion-advection blood flow channels. Moreover, the analysis therein formulates an optimization problem to find the optimal threshold that minimizes the bit error probability (BEP) at the DN. However, a closed-form analytical expression has not been presented for the optimal threshold. The work in [24] analyzed the bit error rate (BER) performance of a dual-hop DF MC system in which the time-dependent molecular concentrations are influenced by the noise and ISI resulting from the channel. In the context of multi-hop communication, the design and analysis of repeater cells for Calcium junction channels was investigated in [25], where signal molecules released by the transmitter are amplified by the intermediate repeaters to reach the receiver. The probability of error analysis for a dual hop system presented in [18] was extended to a multi-hop scenario in [26]. The work in [27] analyzed diffusion based multi-hop MC between bacteria colonies with several bacteria agents combining to act as a single node. Further, a multi-hop system that uses bacteria and virus particles as information carriers was proposed and analyzed in [28] and [29], respectively. However, none of the above works and the references therein consider nanomachine mobility while analyzing the performance of the multiple CN-assisted MC system in diffusion-advection blood flow channels with practical/ realistic effects such as MSI, ISI and counting errors. Moreover, the impact of the detection performance of the intermediate CNs on the end-to-end performance of MC for the aforementioned system has not been analyzed in any of the existing works.

Therefore, this work comprehensively analyzes the impact of intermediate CNs on the performance of a multiple CN-assisted mobile MC system with fully absorbing receivers, with the DF relaying protocol employed at each mobile CN. For this purpose, the LRT-based optimal decision rules and optimal thresholds are determined at each of the mobile CNs and mobile DN in the presence of ISI, MSI, and counting errors, incorporating also the detection performance at each of the previous CNs. Closed-form expressions are subsequently derived for the probabilities of detection and false alarm to analytically characterize the detection performance of the mobile CNs and DN. Finally, the analysis for the end-to-end probability of error and the channel achievable rate is presented for multiple mobile CN-assisted MC between the mobile SN and DN nodes. It is worth mentioning that the results in [1] considering the presence of a single cooperative nanomachine (CN) can be obtained as a special case of the results presented in this paper.

C. Organization

The organization of the rest of the paper is as follows. The system model for the multiple mobile CN-assisted diffusive molecular communication between the mobile SN and mobile DN is presented in Section II. The optimal detection schemes at the mobile CNs and mobile DN are given in Section III. Comprehensive analyses for the probabilities of detection, false alarm at the individual CN, DN, along with the end-to-end probability of error and achievable rate are presented in Section IV, Section V, and Section VI respectively. Simulation results are presented in Section VII, followed by the conclusion in Section VIII.

II. System Model

Consider a multiple CN-assisted MC system inside a blood vessel, i.e., semi-infinite one-dimensional[1] flow-induced fluid medium with constant temperature and viscosity, where the length of the propagation medium is large in comparison to its width. Due to blood flow inside the vessel, the SN, all the CNs and the DN drift with the flow, with $v_{sn} = v_{rn,k} = v_{dn} = v$, where $v_{sn}, v_{rn,k}$ and v_{dn} denote the velocities of the SN, kth CN and DN, respectively, and v denotes the drift velocity of the medium. The diffusion coefficients of the mobile SN, kth mobile CN and the mobile DN are denoted by $D_{sn}, D_{rn,k}$ and D_{dn}, respectively. As described in [40]–[42], the movement of each nanomachine can be modeled as a one dimensional Gaussian random walk where the movement of each nanomachine does not disrupt the propagation of the

[1]Many biological channels such as capillaries, blood vessels and active transportation channels can be modeled by a 1-D drift channel (e.g., [30]–[32]). In particular, they can be modeled as 1-D semi-infinite channels, where the length dimension is significantly larger than the width and height. Also the molecular channels for communication on bio-chips can be approximated by a 1-D environment, since the microfluidic links connecting various components within the chip are very narrow (e.g., [33]). Finally, it is important to note that the 1-D diffusion channel has been frequently applied to investigate several aspects of molecular communications [23], [32], [34]–[39].

information molecules. Moreover, due to the mobility with different diffusion coefficients, the SN, CNs and the DN may pass each other, resulting in different locations of the nanomachines [42].

The communication between the SN and DN occurs in a multiple hop fashion, where the SN and each of the CNs or relays, i.e., $R_1, R_2, \cdots, R_N$, use different types of molecules for transmission. The molecules transmitted by the SN and kth CN propagate via Brownian motion with diffusion coefficient $D_{p,sn}$ and $D_{p,rn,k}$, respectively, in the diffusion-advection blood flow channel. As described in [9], nanomachines such as eukaryotic cells can be genetically modified to emit different types of molecules for transmitting information, thus enabling the intermediate CNs to operate in full duplex mode with simultaneous transmission and reception. The communication takes place over time-slots of duration τ as shown in Fig. 1, where the jth slot is defined as the time interval $[(j-1)\tau, j\tau]$ with $j \in \{1, 2, \cdots\}$. At the beginning of the jth time-slot, the SN emits either $\mathcal{Q}_0$ molecules of type-0 or remains silent, for the transmission of information symbols 1 or 0, respectively, with probabilities β and $1-\beta$. In the subsequent time-slots, the intermediate DF-based CNs first decode the information symbols using the number of molecules received from the previous nanomachine, followed by retransmission to the next nanomachine. The DN finally decodes the information symbol using the number of type-N molecules received from the Nth CN R_N at the end of the $(j+N)$th time-slot. Further, similar to several existing works [15], [23], [43]–[45] and the references therein, this work assumes the nanomachines to be synchronized in time and the transmitted molecules do not interfere or collide with each other. Moreover, once these molecules reach the receiver, they are assumed to be absorbed immediately and not propagate further in the medium. Although, several works on synchronization between static transmitter (TX) and receiver (RX) exist (e.g., [46]), synchronization for the mobile scenario is still not well investigated in the literature. To the best of our knowledge, only the work in [47] considered a synchronization scheme with nanomachine mobility which is applicable only for a fixed TX and mobile RX. Therefore, an interesting future research direction would be to develop new synchronization schemes for molecular communication systems with mobile TX and mobile RX in pure and flow-induced diffusive channels.

Due to the stochastic nature of the diffusive channel, the times of arrival of the molecules emitted by a transmitter nanomachine x, at a receiver nanomachine y, are random in nature, which can span multiple time slots. Let $f_{xy}(t;i)$ denote the probability density function (PDF) of the first hitting time, i.e., the time required for a molecule to reach the nanomachine y. The probability q^{xy}_{j-i}, of a molecule emitted by nanomachine x during slot $i \in \{1, 2, \cdots, j\}$, arriving at nanomachine y during time-slot j, is obtained as [43, Eq. (1)]

$$q^{xy}_{j-i} = \int_{(j-i)\tau}^{(j-i+1)\tau} f_{xy}(t;i)dt. \tag{1}$$

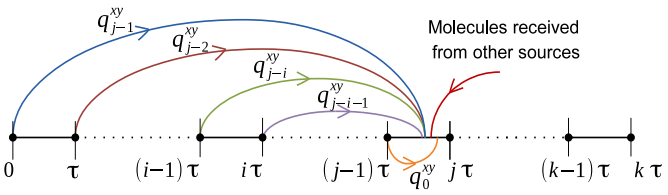

Fig. 1. Time-slotted diffusive MC between two nanomachines x and y.

In a diffusion-advection flow[2] channel, the PDF $f_{xy}(t;i)$, for mobile nanomachines x and y with diffusive coefficients D_x, D_y and $v_x = v_y = v$, is given by [42, Eq. (16)]

$$\begin{aligned} f_{xy}(t;i) =& \frac{\sqrt{i\tau D_{\text{tot}} D_{p,\text{eff}}}}{\pi\sqrt{t(i\tau D_{\text{tot}} + tD_{p,\text{eff}})}} \exp\left(-\frac{(d^0_{xy})^2}{4i\tau D_{\text{tot}}}\right) \\ &+ \frac{d^0_{xy}}{\sqrt{4\pi D_{p,\text{eff}}(t + i\tau D_{\text{tot}}/D_{p,\text{eff}})^3}} \\ &\times \exp\left(-\frac{(d^0_{xy})^2}{4D_{p,\text{eff}}(t + i\tau D_{\text{tot}}/D_{p,\text{eff}})}\right) \\ &\times \text{erf}\left(\frac{d^0_{xy}}{2}\sqrt{\frac{tD_{p,\text{eff}}}{i\tau D_{\text{tot}}(i\tau D_{\text{tot}} + tD_{p,\text{eff}})}}\right), \end{aligned} \tag{2}$$

where d^0_{xy} is the initial Euclidean distance between the nanomachines x and y at time instant $t = 0$, erf$(\cdot)$ denotes the standard error function [48] and the quantities D_{tot} and $D_{p,\text{eff}}$ are defined as, $D_{\text{tot}} = D_x + D_y$ and $D_{p,\text{eff}} = D_y + D_{p,x}$, respectively, where $D_{p,x}$ is the diffusion coefficient of the molecules emitted by the mobile nanomachine x. It is worth noting that the PDF of the first hitting time given in (2) is identical to the PDF of the first hitting time for mobile nanomachines x and y in pure diffusion channels without flow [40, Eq. (6)]. This is due to the fact that the effective flow velocity $v_{\text{eff}} = v - v_y = 0$ since nanomachine y is moving with the flow, i.e., $v_y = v$. A more detailed derivation for the PDF of the first hitting time is given in [42].

The number of type-0 molecules received at R_1 during the jth time-slot $[(j-1)\tau, j\tau]$, corresponding to transmission of the symbol $x[j] \in \{0, 1\}$ by the SN, can be expressed as

$$R_{sr}[j] = S_{sr}[j] + N_{sr}[j] + C_{sr}[j] + \mathcal{I}_{sr}[j], \tag{3}$$

with the various quantities are described as follows. The quantity $S_{sr}[j]$ denotes the number of received molecules corresponding to the transmission in the current slot $[(j-1)\tau, j\tau]$. This follows the Binomial distribution [32], [49] with parameters $\mathcal{Q}_0[j]x[j]$ and q^{sr}_0, i.e., $\mathscr{B}(\mathcal{Q}_0[j]x[j], q^{sr}_0)$, where q^{sr}_0 denotes the probability that a transmitted molecule in a

[2]Similar to several existing works [23], [32], [34]–[39], [45] and the references therein, this work also assumes that neither nanomachines nor molecules have any impact on the flow. This assumption can be justified as follows. First, we assume that the concentration of the information molecules is very low compared to the fluid molecules and hence the transmission of information molecules does not affect the flow profile of the fluidic medium. Second, we also assume that the RX perfectly absorbs the information molecules, but does not influence the fluid molecules, i.e., the flow profile remains constant. This can be accomplished by making the RX sufficiently small. Also, transmitter (TX) is assumed to be a point source. It is worth mentioning that these TX and RX models with constant advection velocity have been frequently considered in 1-D diffusive molecular communication literature, e.g., [23], [32], [34]–[39], [45].

particular slot reaches R_1 within the same slot. The quantity $N_{sr}[j]$ denotes the MSI[3] and follows a Gaussian distribution with mean μ_o and variance σ_o^2 when the number of interfering sources is sufficiently large [50]. The term $C_{sr}[j]$ denotes the counting error pertaining to the molecules received at the CN and can be modeled as a Gaussian distributed random variable with zero mean and variance $\sigma_c^2[j]$. The latter quantity depends on the average number of molecules received at the CN, and is given as $\sigma_c^2[j] = \mathbb{E}\{R_{sr}[j]\}$ [15], [51]. The quantity $\mathcal{I}_{sr}[j]$ is the ISI[4] arising in slot j due to transmissions in the previous $j-1$ slots, which is determined as

$$\mathcal{I}_{sr}[j] = I_{sr}[1] + I_{sr}[2] + \cdots + I_{sr}[j-1], \tag{4}$$

where $I_{sr}[i] \sim \mathscr{B}(\mathcal{Q}_0[j-i]x[j-i], q_i^{sr}), 1 \leq i \leq j-1$, denotes the number of stray molecules received from the transmission of the symbol in the previous $(j-i)$th slot. The parameter q_i^{sr} denotes the probability that a molecule transmitted in $(j-i)$th slot reaches R_1 in the current jth slot. Also, note that the noise $N_{sr}[j]$, the number of molecules received in the current slot $S_{sr}[j]$, and $\mathcal{I}_{sr}[j]$ are independent [15]. The Binomial distribution for $S_{sr}[j]$ can be approximated by the Gaussian distribution[5] with mean $\mu_{sr}[j] = \mathcal{Q}_0[j]x[j]q_0^{sr}$ and variance $\sigma_{sr}^2[j] = \mathcal{Q}_0[j]x[j]q_0^{sr}(1-q_0^{sr})$, i.e., $S_{sr}[j] \sim \mathcal{N}(\mu_{sr}[j], \sigma_{sr}^2[j])$ [52] when the number of molecules released by the SN is sufficiently large. Similarly, the binomial distribution of $I_{sr}[i], 1 \leq i \leq j-1$ can be approximated as

$$I_{sr}[i] \sim \mathcal{N}(\mathcal{Q}_0[j-i]x[j-i]q_i^{sr}, \mathcal{Q}_0[j-i]x[j-i]q_i^{sr}(1-q_i^{sr})).$$

Further, note that the terms $S_{sr}[j]$ and $I_{sr}[i], i = 1, 2, \cdots, j-1$ are independent since the molecules transmitted in different time-slots do not interfere with each other [15], [23].

Consider now any intermediate CN R_{n+1} corresponding to $n = 1, 2, \cdots, N-1$. The number of molecules received at R_{n+1} corresponding to the transmission of $\widehat{x}[j+n-1] \in \{0,1\}$ by the previous hop CN R_n, emitting $\mathcal{Q}_n[j+n]$ molecules, during the time-slot $[(j+n-1)\tau, (j+n)\tau]$ can be expressed as

$$\begin{aligned} R_{rr}[j+n] =& S_{rr}[j+n] + N_{rr}[j+n] + C_{rr}[j+n] \\ &+ \mathcal{I}_{rr}[j+n], \end{aligned} \tag{5}$$

where $S_{rr}[j+n] \sim \mathcal{N}(\mathcal{Q}_n[j+n]\widehat{x}[j+n-1]q_0^{rr}, \mathcal{Q}_n[j+n]\widehat{x}[j+n-1]q_0^{rr}(1-q_0^{rr}))$ is the number of type-n molecules that are received by R_{n+1} in the current slot $[(j+n-1)\tau, (j+n)\tau]$ which is transmitted by R_n in the same slot. The quantity $N_{rr}[j+n] \sim \mathcal{N}(\mu_o, \sigma_o^2)$ is the MSI at R_{n+1} arising due to molecules received from the other sources. The term $C_{rr}[j+n] \sim \mathcal{N}(0, \mathbb{E}\{R_{rr}[j+n]\})$ denotes the counting errors, while $\mathcal{I}_{rr}[j+n]$ represents the ISI at R_{n+1} that is given as $\mathcal{I}_{rr}[j+n] = \sum_{i=n+1}^{j+n-1} I_{rr}[i]$, with $I_{rr}[i]$ distributed as $I_{rr}[i] \sim \mathcal{N}(\mathcal{Q}_n[j+2n-i]\widehat{x}[j+2n-i-1]q_{i-n}^{rr}, \mathcal{Q}_n[j+2n-i]\widehat{x}[j+2n-i-1]q_{i-n}^{rr}(1-q_{i-n}^{rr}))$, $n+1 \leq i \leq j+n-1$. Note that $I_{rr}[i]$ denotes the number of stray molecules received due to transmission in the previous $(j+2n-i)$th slot. The number of molecules received at the DN, corresponding to the transmission by the last CN R_N using $\mathcal{Q}_N[j+N]$, during the time slot $[(j+N-1)\tau, (j+N)\tau]$, can be expressed as

$$\begin{aligned} R_{rd}[j+N] =& S_{rd}[j+N] + \mathcal{I}_{rd}[j+N] + N_{rd}[j+N] \\ &+ C_{rd}[j+N], \end{aligned} \tag{6}$$

where $S_{rd}[j+N]$ follows the distribution

$$S_{rd}[j+N] \sim \mathcal{N}(\mathcal{Q}_N[j+N]\widehat{x}[j+N-1]q_0^{rd}, \mathcal{Q}_N[j+N]\widehat{x}[j+N-1]q_0^{rd}(1-q_0^{rd})).$$

The quantities $N_{rd}[j+N] \sim \mathcal{N}(\mu_o, \sigma_o^2)$ and $C_{rd}[j+N] \sim \mathcal{N}(0, \mathbb{E}\{R_{rd}[j+N]\})$ denote the MSI and counting errors, respectively, at the DN. Similarly, the ISI component $\mathcal{I}_{rd}[j+N]$ at the DN is $\mathcal{I}_{rd}[j+N] = \sum_{i=N+1}^{j+N-1} I_{rd}[i]$, where $I_{rd}[i], N+1 \leq i \leq j+N-1$ is distributed as

$$I_{rd}[i] \sim \mathcal{N}(\mathcal{Q}_N[j+2N-i]\widehat{x}[j+2N-i-1]q_{i-N}^{rd}, \mathcal{Q}_N[j+2N-i]\widehat{x}[j+2N-i-1]q_{i-N}^{rd}(1-q_{i-N}^{rd})).$$

The optimal decision rules at each of the receiving nanomachines, i.e., all the CNs and the DN, are derived in the next section followed by a comprehensive analysis of the resulting probabilities of detection and false alarm, probability of error, and end-to-end achievable rate.

III. Detection Schemes at the DN and each CN

A. Optimal Decision Rule at the First CN

Using the model in (3), the problem for symbol detection at R_1 can be formulated as the binary hypothesis testing problem

$$\begin{aligned} \mathcal{H}_0 : R_{sr}[j] =& \mathcal{I}_{sr}[j] + N_{sr}[j] + C_{sr}[j] \\ \mathcal{H}_1 : R_{sr}[j] =& S_{sr}[j] + \mathcal{I}_{sr}[j] + N_{sr}[j] + C_{sr}[j], \end{aligned} \tag{7}$$

where the hypotheses $\mathcal{H}_0$ and $\mathcal{H}_1$ above correspond to the transmission of binary symbols 0 and 1, respectively, by the SN, during the jth time-slot. The number of molecules $R_{sr}[j]$ received at R_1, corresponding to the individual hypotheses, are distributed as

$$\begin{aligned} \mathcal{H}_0 : R_{sr}[j] &\sim \mathcal{N}(\mu_{sr,0}[j], \sigma_{sr,0}^2[j]) \\ \mathcal{H}_1 : R_{sr}[j] &\sim \mathcal{N}(\mu_{sr,1}[j], \sigma_{sr,1}^2[j]), \end{aligned} \tag{8}$$

where the means $\mu_{sr,0}[j]$, $\mu_{sr,1}[j]$ and variances $\sigma_{sr,0}^2[j]$, $\sigma_{sr,1}^2[j]$ corresponding to hypotheses $\mathcal{H}_0$, $\mathcal{H}_1$, respectively, can be obtained starting with the expression in (3) and are determined as given below

$$\mu_{sr,0}[j] = \beta \sum_{i=1}^{j-1} \mathcal{Q}_0[j-i]q_i^{sr} + \mu_o, \tag{9}$$

$$\mu_{sr,1}[j] = \mathcal{Q}_0[j]q_0^{sr} + \mu_{sr,0}[j], \tag{10}$$

$$\sigma_{sr,0}^2[j] = \sum_{i=1}^{j-1} \{\beta\mathcal{Q}_0[j-i]q_i^{sr}(1-q_i^{sr}) + \beta(1-\beta) \times (\mathcal{Q}_0[j-i]q_i^{sr})^2\} + \sigma_o^2 + \mu_{sr,0}[j], \tag{11}$$

$$\sigma_{sr,1}^2[j] = \mathcal{Q}_0[j]q_0^{sr}(2-q_0^{sr}) + \sigma_{sr,0}^2[j]. \tag{12}$$

[3]Multi-source interference (MSI) arises from the transmissions of other sources that use the same type of molecules. Also, note that this work considers a worst case scenario where each of the CNs and the DN experience the interference from other sources existing in the same medium.

[4]Inter-symbol interference (ISI) at the receiving nanomachine arises due to Brownian motion, which results in a fraction of the molecules emitted by the transmitting nanomachine at the beginning of a given time-slot, arriving randomly in later time-slots.

[5]This approximation is reasonable when $\mathcal{Q}_0[j]q_0^{sr} > 5$ and $\mathcal{Q}_0[j](1-q_0^{sr}) > 5$ [15].

Using the PDFs for $p(R_{sr}[j]|\mathcal{H}_0)$ and $p(R_{sr}[j]|\mathcal{H}_1)$ stated in (8), the following result presents the LRT-based optimal decision rule at R_1 for symbol detection.

Theorem 1: The LRT-based optimal decision rule at R_1 corresponding to transmission by the SN, during the jth time-slot $[(j-1)\tau, j\tau]$, is obtained as

$$T(R_{sr}[j]) = R_{sr}[j] \underset{\mathcal{H}_0}{\overset{\mathcal{H}_1}{\gtrless}} \gamma'_{sr}[j], \tag{13}$$

where $\gamma'_{sr}[j]$ is the optimal decision threshold defined as $\gamma'_{sr}[j] = \sqrt{\gamma_{sr}[j]} - \alpha_{sr}[j]$ with the quantities $\gamma_{sr}[j]$ and $\alpha_{sr}[j]$ given as

$$\alpha_{sr}[j] = \frac{\mu_{sr,1}[j]\sigma^2_{sr,0}[j] - \mu_{sr,0}[j]\sigma^2_{sr,1}[j]}{\sigma^2_{sr,1}[j] - \sigma^2_{sr,0}[j]}. \tag{14}$$

$$\gamma_{sr}[j] = \frac{2\sigma^2_{sr,1}[j]\sigma^2_{sr,0}[j]}{\sigma^2_{sr,1}[j] - \sigma^2_{sr,0}[j]} \ln\left[\frac{(1-\beta)}{\beta}\sqrt{\frac{\sigma^2_{sr,1}[j]}{\sigma^2_{sr,0}[j]}}\right] + (\alpha_{sr}[j])^2 + \frac{\mu^2_{sr,1}[j]\sigma^2_{sr,0}[j] - \mu^2_{sr,0}[j]\sigma^2_{sr,1}[j]}{\sigma^2_{sr,1}[j] - \sigma^2_{sr,0}[j]}. \tag{15}$$

Proof: The log likelihood ratio test (LLRT) at R_1 is obtained as

$$\Lambda(R_{sr}[j]) = \ln\left[\frac{p(R_{sr}[j]|\mathcal{H}_1)}{p(R_{sr}[j]|\mathcal{H}_0)}\right] \underset{\mathcal{H}_0}{\overset{\mathcal{H}_1}{\gtrless}} \ln\left[\frac{1-\beta}{\beta}\right]. \tag{16}$$

On substituting the expressions for the PDFs $p(R_{sr}[j]|\mathcal{H}_1)$ and $p(R_{sr}[j]|\mathcal{H}_0)$ obtained in (8) in the above equation, followed by simplification, the test statistic $\Lambda(R_{sr}[j])$ reduces to

$$\Lambda(R_{sr}[j]) = \ln\sqrt{\frac{\sigma^2_{sr,0}[j]}{\sigma^2_{sr,1}[j]}} + \frac{1}{2\sigma^2_{sr,0}[j]\sigma^2_{sr,1}[j]} f(R_{sr}[j]), \tag{17}$$

where the quantity $f(R_{sr}[j])$ above is defined in (18) and can be further simplified as shown below

$$\begin{aligned} &f(R_{sr}[j]) \\ &\triangleq (R_{sr}[j]-\mu_{sr,0}[j])^2\sigma^2_{sr,1}[j] - (R_{sr}[j]-\mu_{sr,1}[j])^2\sigma^2_{sr,0}[j] \\ &= R^2_{sr}[j](\sigma^2_{sr,1}[j]-\sigma^2_{sr,0}[j]) + \mu^2_{sr,0}[j]\sigma^2_{sr,1}[j] - \mu^2_{sr,1}[j]\sigma^2_{sr,0}[j] \\ &\quad + 2R_{sr}[j](\mu_{sr,1}[j]\sigma^2_{sr,0}[j] - \mu_{sr,0}[j]\sigma^2_{sr,1}[j]) \\ &= (\sigma^2_{sr,1}[j] - \sigma^2_{sr,0}[j])(R_{sr}[j] + \alpha_{sr}[j])^2 + \mu^2_{sr,0}[j]\sigma^2_{sr,1}[j] \\ &\quad - \mu^2_{sr,1}[j]\sigma^2_{sr,0}[j] - (\mu_{sr,1}[j]\sigma^2_{sr,0}[j] - \mu_{sr,0}[j]\sigma^2_{sr,1}[j])\alpha_{sr}[j], \end{aligned} \tag{18}$$

with the quantity $\alpha_{sr}[j]$ as given in (14). Substituting the above expression for $f(R_{sr}[j])$ in (17) followed by merging the terms independent of the received molecules $R_{sr}[j]$ with the threshold on the right hand side of the test, the LLRT reduces to

$$(R_{sr}[j] + \alpha_{sr}[j])^2 \underset{\mathcal{H}_0}{\overset{\mathcal{H}_1}{\gtrless}} \gamma_{sr}[j], \tag{19}$$

where the decision threshold $\gamma_{sr}[j]$ is as stated in (15) in Theorem 1. It can be readily observed from (10) and (12) that $\alpha_{sr}[j] \geq 0$ and $\gamma_{sr}[j] \geq 0$ are non-negative, which arises due to the fact that $\mu_{sr,1}[j] > \mu_{sr,0}[j]$ and $\sigma^2_{sr,1}[j] > \sigma^2_{sr,0}[j]$. Hence, considering the square root of the test statistic in (19) yields the optimal test given in (13) of Theorem 1. ■

B. Optimal Decision Rule at the DN

The symbol detection problem at the DN corresponding to the transmission by R_N in the $(j+N)$th time-slot can be formulated as the binary hypothesis testing problem

$$\begin{aligned} \mathcal{H}_0 : R_{rd}[j+N] &= \mathcal{I}_{rd}[j+N] + N_{rd}[j+N] \\ &\quad + C_{rd}[j+N] \\ \mathcal{H}_1 : R_{rd}[j+N] &= S_{rd}[j+N] + \mathcal{I}_{rd}[j+N] \\ &\quad + N_{rd}[j+N] + C_{rd}[j+N], \end{aligned} \tag{20}$$

where $\mathcal{H}_0$ and $\mathcal{H}_1$ denote the null and alternative hypotheses corresponding to the transmission of the decoded symbols $\widehat{x}[j+N-1] = 0$ and $\widehat{x}[j+N-1] = 1$, respectively, by the R_N in the $(j+N)$th time slot. The distributions of $R_{rd}[j+N]$ corresponding to the two hypotheses in (20) can be determined as

$$\begin{aligned} \mathcal{H}_0 : R_{rd}[j+N] &\sim \mathcal{N}(\mu_{rd,0}[j+N], \sigma^2_{rd,0}[j+N]) \\ \mathcal{H}_1 : R_{rd}[j+N] &\sim \mathcal{N}(\mu_{rd,1}[j+N], \sigma^2_{rd,1}[j+N]), \end{aligned} \tag{21}$$

where the mean $\mu_{rd,0}[j+N]$ and variance $\sigma^2_{rd,0}[j+N]$ under the null hypothesis $\mathcal{H}_0$ are [41, Appendix A]

$$\mu_{rd,0}[j+N] = \beta \sum_{i=N+1}^{j+N-1} \mathcal{Q}_N[j+2N-i] q^{rd}_{i-N} + \mu_o, \tag{22}$$

$$\begin{aligned} \sigma^2_{rd,0}[j+N] = \sum_{i=N+1}^{j+N-1} &[\beta\mathcal{Q}_N[j+2N-i]q^{rd}_{i-N}(1-q^{rd}_{i-N}) + \beta \\ &\times (1-\beta)(\mathcal{Q}_N[j+2N-i]q^{rd}_{i-N})^2] \\ &+ \sigma^2_o + \mu_{rd,0}[j+N]. \end{aligned} \tag{23}$$

Similarly, the mean $\mu_{rd,1}[j+1]$ and variance $\sigma^2_{rd,1}[j+1]$ corresponding to the alternative hypothesis $\mathcal{H}_1$ are [41, Appendix B]

$$\mu_{rd,1}[j+N] = \mathcal{Q}_N[j+N] q^{rd}_0 + \mu_{rd,0}[j+N], \tag{24}$$

$$\sigma^2_{rd,1}[j+N] = \mathcal{Q}_N[j+N] q^{rd}_0 (2 - q^{rd}_0) + \sigma^2_{rd,0}[j+1]. \tag{25}$$

Using the PDFs obtained in (21), the optimal test at the DN is given below.

Theorem 2: The optimal detector at the DN, for the multiple CN-assisted diffusive mobile molecular communication system, corresponding to the transmission by R_N in the $(j+N)$th time-slot, is given by

$$T(R_{rd}[j+N]) = R_{rd}[j+N] \underset{\mathcal{H}_0}{\overset{\mathcal{H}_1}{\gtrless}} \gamma'_{rd}[j+N], \tag{26}$$

where the optimal decision threshold $\gamma'_{rd}[j+N]$ is given as,

$$\gamma'_{rd}[j+N] = \sqrt{\gamma_{rd}[j+N]} - \alpha_{rd}[j+N], \tag{27}$$

with the quantity $\alpha_{rd}[j+N]$ defined as

$$\alpha_{rd}[j+N] = \frac{\mu_{rd,1}[j+N]\sigma^2_{rd,0}[j+N] - \mu_{rd,0}[j+N]\sigma^2_{rd,1}[j+N]}{\sigma^2_{rd,1}[j+N] - \sigma^2_{rd,0}[j+N]}. \tag{28}$$

The expression for $\gamma_{rd}[j+N]$ is given in (29), where the

$$\gamma_{rd}[j+N] = \ln\left[\sqrt{\frac{\sigma^2_{rd,1}[j+N]}{\sigma^2_{rd,0}[j+N]}}\beta_{rd}\right]\frac{2\sigma^2_{rd,1}[j+N]\sigma^2_{rd,0}[j+N]}{\sigma^2_{rd,1}[j+N]-\sigma^2_{rd,0}[j+N]}+(\alpha_{rd}[j+N])^2 + \frac{\mu^2_{rd,1}[j+N]\sigma^2_{rd,0}[j+N]-\mu^2_{rd,0}[j+N]\sigma^2_{rd,1}[j+N]}{\sigma^2_{rd,1}[j+N]-\sigma^2_{rd,0}[j+N]}, \quad (29)$$

quantity β_{rd} is defined as

$$\beta_{rd}=\frac{(1-\beta)(1-P^{(N)}_{FA}[j+N-1])-\beta(1-P^{(N)}_{D}[j+N-1])}{\beta P^{(N)}_{D}[j+N-1]-(1-\beta)P^{(N)}_{FA}[j+N-1]}. \quad (30)$$

Proof: Given in Appendix A. ∎

It is worth noticing that the optimal decision threshold in (27) of Theorem 2 additionally depends on the detection performance of R_N, i.e., probability of detection $P^{(N)}_D[j+N-1]$ and probability of false alarm $P^{(N)}_{FA}[j+N-1]$. In contrast to the results obtained above for the DN, the decision rule at R_1 in Theorem 1 does not depend on the detection performance of any other CNs as it directly communicates with the SN. Further, on the similar lines given in Appendix A, one can also readily derive the optimal decision rules for symbol detection at the intermediate CNs $R_{n+1}, n = 1, 2, \cdots, N-1$, corresponding to the transmission by R_n in $(j+n-1)$th time slot.

IV. Detection Performance Analysis

This section characterizes the detection performance at the various nodes in the multiple CN-assisted diffusive mobile molecular communication system. Result below gives the expressions for the resulting probabilities of detection and false alarm at the DN.

Theorem 3: The average probabilities of detection P_D and false alarm P_{FA} at the DN corresponding to the transmission by the SN in slots 1 to k, in the multiple CN-assisted diffusion-advection flow molecular communication system with mobile nanomachines, are given as

$$P_D = \frac{1}{k}\sum_{j=1}^{k} P^d_D[j+N], \quad P_{FA} = \frac{1}{k}\sum_{j=1}^{k} P^d_{FA}[j+N], \quad (31)$$

where the probabilities of detection $P^d_D[j+N]$ and false alarm $P^d_{FA}[j+N]$ at the DN, in the $(j+N)$th slot, are given as

$$\begin{aligned} &P^d_D[j+N] \\ &= Q\left(\frac{\gamma'_{rd}[j+N]-\mu_{rd,0}[j+N]}{\sigma_{rd,0}[j+N]}\right)\left(1-P^{(N)}_D[j+N-1]\right) \\ &\quad + Q\left(\frac{\gamma'_{rd}[j+N]-\mu_{rd,1}[j+N]}{\sigma_{rd,1}[j+N]}\right)P^{(N)}_D[j+N-1], \quad (32) \\ &P^d_{FA}[j+N] \\ &= Q\left(\frac{\gamma'_{rd}[j+N]-\mu_{rd,0}[j+N]}{\sigma_{rd,0}[j+N]}\right)\left(1-P^{(N)}_{FA}[j+N-1]\right) \\ &\quad + Q\left(\frac{\gamma'_{rd}[j+N]-\mu_{rd,1}[j+N]}{\sigma_{rd,1}[j+N]}\right)P^{(N)}_{FA}[j+N-1]. \quad (33) \end{aligned}$$

The threshold $\gamma'_{rd}[j+N]$ is as defined in (27) and the Q-function $Q(\cdot)$ denotes the tail probability of the standard Normal random variable.

Proof: The probability of detection $P^d_D[j+N]$ at the DN, corresponding to the transmission by R_N in the $(j+N)$th slot, can be derived using the test statistic $T(R_{rd}[j+N])$ given in (26) as

$$\begin{aligned} &P^d_D[j+N] \\ &= \Pr(T(R_{rd}[j+N]) > \gamma'_{rd}[j+N]|\mathcal{H}_1) \\ &= \sum_{l=0}^{2^N-1} \Pr(R_{rd}[j+N] > \gamma'_{rd}[j+N]|\xi_l)\Pr(\xi_l|\mathcal{H}_1), \quad (34) \end{aligned}$$

where $\Pr(\xi_l|\mathcal{H}_1)$ is given in (64) and $\Pr(R_{rd}[j+N] > \gamma'_{rd}[j+N]|\xi_l)$ can be obtained using (59) as

$$\begin{aligned} &\Pr(R_{rd}[j+N] > \gamma'_{rd}[j+N]|\xi_l) \\ &= \begin{cases} Q\left(\frac{\gamma'_{rd}[j+N]-\mu_{rd,0}[j+N]}{\sigma_{rd,0}[j+N]}\right) & \text{if } l = 0, 2, \cdots, 2^N-2 \\ Q\left(\frac{\gamma'_{rd}[j+N]-\mu_{rd,1}[j+N]}{\sigma_{rd,1}[j+N]}\right) & \text{if } l = 1, 3, \cdots, 2^N-1. \end{cases} \quad (35) \end{aligned}$$

Finally, employing the results in (64) and (35) in (34), the expression for $P^d_D[j+N]$ is obtained as

$$\begin{aligned} &P^d_D[j+N] \\ &= \sum_{l=0,2,\cdots,2^N-2} Q\left(\frac{\gamma'_{rd}[j+N]-\mu_{rd,0}[j+N]}{\sigma_{rd,0}[j+N]}\right) \\ &\quad \times \left[\prod_{n\in\Psi^1_l} P^{(n)}_D[j+n-1] \prod_{n\in\bar{\Psi}^1_l}\left(1-P^{(n)}_D[j+n-1]\right)\right] \\ &\quad + \sum_{l=1,3,\cdots,2^N-1} Q\left(\frac{\gamma'_{rd}[j+N]-\mu_{rd,1}[j+N]}{\sigma_{rd,1}[j+N]}\right) \\ &\quad \times \left[\prod_{n\in\Psi^1_l} P^{(n)}_D[j+n-1] \prod_{n\in\bar{\Psi}^1_l}\left(1-P^{(n)}_D[j+n-1]\right)\right]. \quad (36) \end{aligned}$$

Considering the 2^N possible states ξ_l for the N CNs and the corresponding sets $\Psi^1_l, \bar{\Psi}^1_l$, the above expression for $P^d_D[j+N]$ reduces to the one stated in (32), where the following results have been used in the simplification process

$$\begin{aligned} &\sum_{l=0,2,\cdots,2^N-2}\left[\prod_{n\in\Psi^1_l} P^{(n)}_D[j+n-1] \prod_{n\in\bar{\Psi}^1_l}\left(1-P^{(n)}_D[j+n-1]\right)\right] \\ &\quad = 1 - P^{(N)}_D[j+N-1], \quad (37) \end{aligned}$$

and

$$\begin{aligned} &\sum_{l=1,3,\cdots,2^N-1}\left[\prod_{n\in\Psi^1_l} P^{(n)}_D[j+n-1] \prod_{n\in\bar{\Psi}^1_l}\left(1-P^{(n)}_D[j+n-1]\right)\right] \\ &\quad = P^{(N)}_D[j+N-1]. \quad (38) \end{aligned}$$

For instance, the above results can be readily verified for a system with $N = 2$ CNs as follows

$$\sum_{l=0,2}\left[\prod_{n\in\Psi_l^1}P_D^{(n)}[j+n-1]\prod_{n\in\bar{\Psi}_l^1}\left(1-P_D^{(n)}[j+n-1]\right)\right]$$
$$=\left(1-P_D^{(1)}[j]\right)\left(1-P_D^{(2)}[j+1]\right)+P_D^{(1)}[j]\left(1-P_D^{(2)}[j+1]\right)$$
$$=1-P_D^{(2)}[j+1],$$
$$\sum_{l=1,3}\left[\prod_{n\in\Psi_l^1}P_D^{(n)}[j+n-1]\prod_{n\in\bar{\Psi}_l^1}\left(1-P_D^{(n)}[j+n-1]\right)\right]$$
$$=\left(1-P_D^{(1)}[j]\right)P_D^{(2)}[j+1]+P_D^{(1)}[j]P_D^{(2)}[j+1]$$
$$=P_D^{(2)}[j+1].$$

Similarly, the probability of false alarm $P_{FA}^d[j+N]$ at the DN, in the $(j+N)$th slot, can be derived as

$$P_{FA}^d[j+N]$$
$$=\Pr(T(R_{rd}[j+N])>\gamma'_{rd}[j+N]|\mathcal{H}_0)$$
$$=\sum_{l=0}^{2^N-1}\Pr(R_{rd}[j+N]>\gamma'_{rd}[j+N]|\xi_l)\Pr(\xi_l|\mathcal{H}_0). \quad (39)$$

Further, substituting the expressions for $\Pr(\xi_l|\mathcal{H}_0)$ from (63) and $\Pr(R_{rd}[j+N] > \gamma'_{rd}[j+N]|\xi_l)$ from (35) in (39), the expression for $P_{FA}^d[j+N]$ follows as

$$P_{FA}^d[j+N]$$
$$=\sum_{l=0,2,\cdots,2^N-2}Q\left(\frac{\gamma'_{rd}[j+N]-\mu_{rd,0}[j+N]}{\sigma_{rd,0}[j+N]}\right)$$
$$\times\left[\prod_{n\in\Psi_l^0}P_{FA}^{(n)}[j+n-1]\prod_{n\in\bar{\Psi}_l^0}\left(1-P_{FA}^{(n)}[j+n-1]\right)\right]$$
$$+\sum_{l=1,3,\cdots,2^N-1}Q\left(\frac{\gamma'_{rd}[j+N]-\mu_{rd,1}[j+N]}{\sigma_{rd,1}[j+N]}\right)$$
$$\times\left[\prod_{n\in\Psi_l^0}P_{FA}^{(n)}[j+n-1]\prod_{n\in\bar{\Psi}_l^0}\left(1-P_{FA}^{(n)}[j+n-1]\right)\right]. \quad (40)$$

Considering the 2^N possible states ξ_l similar to (37) and (38), one can demonstrate the results below

$$\sum_{l=0,2,\cdots,2^N-2}\left[\prod_{n\in\Psi_l^0}P_{FA}^{(n)}[j+n-1]\prod_{n\in\bar{\Psi}_l^0}\left(1-P_{FA}^{(n)}[j+n-1]\right)\right]$$
$$=1-P_{FA}^{(N)}[j+N-1], \quad (41)$$

and

$$\sum_{l=1,3,\cdots,2^N-1}\left[\prod_{n\in\Psi_l^0}P_{FA}^{(n)}[j+n-1]\prod_{n\in\bar{\Psi}_l^0}\left(1-P_{FA}^{(n)}[j+n-1]\right)\right]$$
$$=P_{FA}^{(N)}[j+N-1]. \quad (42)$$

Substituting these results in equation (40) above yields the desired result for $P_{FA}^d[j+N]$ stated in (33). ■

A. *Probabilities of Detection and False Alarm at CNs*

The probabilities of detection $P_D^{(n+1)}[j+n]$ and false alarm $P_{FA}^{(n+1)}[j+n]$ at R_{n+1}, corresponding to the transmission by R_n in the $(j+n)$th slot, can be described in terms of the test statistic $T(R_{rr}[j+n]) = R_{rr}[j+n] \underset{\mathcal{H}_0}{\overset{\mathcal{H}_1}{\gtrless}} \gamma'_{rr}[j+n]$ as

$$P_D^{(n+1)}[j+n]$$
$$=\Pr(T(R_{rr}[j+n])>\gamma'_{rr}[j+n]|\mathcal{H}_1)$$
$$=\sum_{l=0}^{2^n-1}\Pr(R_{rr}[j+n]>\gamma'_{rr}[j+n]|\xi_l)\Pr(\xi_l|\mathcal{H}_1), \quad (43)$$

$$P_{FA}^{(n+1)}[j+n]$$
$$=\Pr(T(R_{rr}[j+n])>\gamma'_{rr}[j+n]|\mathcal{H}_0)$$
$$=\sum_{l=0}^{2^n-1}\Pr(R_{rr}[j+n]>\gamma'_{rr}[j+n]|\xi_l)\Pr(\xi_l|\mathcal{H}_0), \quad (44)$$

where $\gamma'_{rr}[j+n]$ is the optimal decision threshold at R_{n+1}. The above expressions for $P_D^{(n+1)}[j+n]$ and $P_{FA}^{(n+1)}[j+n]$ can be simplified along lines similar to the proof of Theorem 3 to yield

$$P_D^{(n+1)}[j+n]$$
$$=\sum_{l=0,2,\cdots,2^n-2}Q\left(\frac{\gamma'_{rr}[j+n]-\mu_{rr,0}[j+n]}{\sigma_{rr,0}[j+n]}\right)$$
$$\times\left[\prod_{n\in\Psi_l^1}P_D^{(n)}[j+n-1]\prod_{n\in\bar{\Psi}_l^1}\left(1-P_D^{(n)}[j+n-1]\right)\right]$$
$$+\sum_{l=1,3,\cdots,2^n-1}Q\left(\frac{\gamma'_{rr}[j+n]-\mu_{rr,1}[j+n]}{\sigma_{rr,1}[j+n]}\right)$$
$$\times\left[\prod_{n\in\Psi_l^1}P_D^{(n)}[j+n-1]\prod_{n\in\bar{\Psi}_l^1}\left(1-P_D^{(n)}[j+n-1]\right)\right]$$
$$=Q\left(\frac{\gamma'_{rr}[j+n]-\mu_{rr,0}[j+n]}{\sigma_{rr,0}[j+n]}\right)\left(1-P_D^{(n)}[j+n-1]\right)$$
$$+Q\left(\frac{\gamma'_{rr}[j+n]-\mu_{rr,1}[j+n]}{\sigma_{rr,1}[j+n]}\right)P_D^{(n)}[j+n-1]. \quad (45)$$

$$P_{FA}^{(n+1)}[j+n]$$
$$=\sum_{l=0,2,\cdots,2^n-2}Q\left(\frac{\gamma'_{rr}[j+n]-\mu_{rr,0}[j+n]}{\sigma_{rr,0}[j+n]}\right)$$
$$\times\left[\prod_{n\in\Psi_l^0}P_{FA}^{(n)}[j+n-1]\prod_{n\in\bar{\Psi}_l^0}\left(1-P_{FA}^{(n)}[j+n-1]\right)\right]$$
$$+\sum_{l=1,3,\cdots,2^n-1}Q\left(\frac{\gamma'_{rr}[j+n]-\mu_{rr,1}[j+n]}{\sigma_{rr,1}[j+n]}\right)$$
$$\times\left[\prod_{n\in\Psi_l^0}P_{FA}^{(n)}[j+n-1]\prod_{n\in\bar{\Psi}_l^0}\left(1-P_{FA}^{(n)}[j+n-1]\right)\right]$$
$$=Q\left(\frac{\gamma'_{rr}[j+n]-\mu_{rr,0}[j+n]}{\sigma_{rr,0}[j+n]}\right)\left(1-P_{FA}^{(n)}[j+n-1]\right)$$
$$+Q\left(\frac{\gamma'_{rr}[j+n]-\mu_{rr,1}[j+n]}{\sigma_{rr,1}[j+n]}\right)P_{FA}^{(n)}[j+n-1]. \quad (46)$$

V. Bit-Error Probability Analysis

The end-to-end probability of bit-error for the multiple CN-assisted MC process between the SN and DN is given by the result below.

Theorem 4: The average probability of error (P_e) at the DN corresponding to transmission by the SN in slots 1 to k is given as

$$P_e=\frac{1}{k}\sum_{j=1}^{k}\Big\{\big(1-P_D^d[j+N]\big)\,\beta+P_{FA}^d[j+N](1-\beta)\Big\}, \quad (47)$$

where β denotes the prior probability of the hypothesis $\mathcal{H}_1$ and the expressions for the probabilities $P_D^d[j+N]$ and $P_F^d[j+N]$ are determined in (32) and (33).

Proof: The average probability of error P_e for slots 1 to k can be expressed as

$$P_e=\frac{1}{k}\sum_{j=1}^{k}P_e^d[j+N], \quad (48)$$

where $P_e^d[j+N]$ denotes the probability of error at the DN in slot $j+N$, corresponding to the transmission by the SN in slot j. The quantity $P_e^d[j+N]$ can be derived as [41], [53]

$$\begin{aligned}&P_e^d[j+N]\\&=\text{Pr(decide }\mathcal{H}_0,\mathcal{H}_1\text{ true)}+\text{Pr(decide }\mathcal{H}_1,\mathcal{H}_0\text{ true)}\\&=(1-P_D^d[j+N])\text{Pr}(\mathcal{H}_1)+P_{FA}^d[j+N]\text{Pr}(\mathcal{H}_0)\\&=(1-P_D^d[j+N])\beta+P_{FA}^d[j+N](1-\beta). \quad (49)\end{aligned}$$

Substituting the above expression for $P_e^d[j+N]$ in (48) yields the desired result for P_e as stated in (47). ■

Remark: The average probability of error (P_e) for a single CN-assisted dual-hop system considered in [1] can now be readily obtained by substituting $N=1$ in the above result as

$$P_e=\frac{1}{k}\sum_{j=1}^{k}\Big\{\big(1-P_D^d[j+1]\big)\,\beta+P_{FA}^d[j+1](1-\beta)\Big\}, \quad (50)$$

where the expressions for the probabilities $P_D^d[j+1]$ and $P_F^d[j+1]$ for the CN $N=1$ can be obtained using (32) and (33) as

$$\begin{aligned}P_D^d[j+1]=&Q\left(\frac{\gamma'_{rd}[j+1]-\mu_{rd,0}[j+1]}{\sigma_{rd,0}[j+1]}\right)(1-P_D^{(1)}[j])\\&+Q\left(\frac{\gamma'_{rd}[j+1]-\mu_{rd,1}[j+1]}{\sigma_{rd,1}[j+1]}\right)P_D^{(1)}[j], \quad (51)\\P_{FA}^d[j+1]=&Q\left(\frac{\gamma'_{rd}[j+1]-\mu_{rd,0}[j+1]}{\sigma_{rd,0}[j+1]}\right)(1-P_{FA}^{(1)}[j])\\&+Q\left(\frac{\gamma'_{rd}[j+1]-\mu_{rd,1}[j+1]}{\sigma_{rd,1}[j+1]}\right)P_{FA}^{(1)}[j], \quad (52)\end{aligned}$$

where the probabilities of detection $(P_D^{(1)}[j])$ and false alarm $(P_{FA}^{(1)}[j])$ at the intermediate CN are obtained using the test in (13) as

$$\begin{aligned}P_D^{(1)}[j]&=Q\left(\frac{\gamma_{sr}[j]-\mu_{sr,1}[j]}{\sigma_{sr,1}[j]}\right), \quad (53)\\P_{FA}^{(1)}[j]&=Q\left(\frac{\gamma_{sr}[j]-\mu_{sr,0}[j]}{\sigma_{sr,0}[j]}\right). \quad (54)\end{aligned}$$

TABLE I
Simulation Parameters

Parameter	Value
Diffusion coefficient D_p [40]	5×10^{-10} m^2/s
Drift velocity v [54], [55]	1×10^{-3} m/s
Slot duration τ [3]	10 ms
Number of molecules emitted for symbol 1	30, 60, 100
MSI noise mean μ_o and variance σ_o^2 [1]	10
Prior probability β	0.5

Further, note that the above expressions (53) and (54) can also be used along with (32), (33) , (45), (46) in (31) to analyze the end-to-end error performance of the systems with $N\geq 2$ CNs.

VI. Achievable Rate Analysis

Let the discrete random variables $X[j]$ and $Y[j+N]$ represent the transmitted and received symbol in the jth and $(j+N)$th slots, respectively. The mutual information $I(X[j],Y[j+N])$ between $X[j]$ and $Y[j+N]$ for the multiple CN-assisted link can be expressed as

$$\begin{aligned}&I(X[j],Y[j+N])\\&=\text{Pr}(y[j+N]=0|x[j]=0)\text{Pr}(x[j]=0)\\&\quad\times\log_2\frac{\text{Pr}(y[j+N]=0|x[j]=0)}{\sum_{x[j]\in\{0,1\}}\text{Pr}(y[j+N]=0|x[j])\text{Pr}(x[j])}\\&\quad+\text{Pr}(y[j+N]=0|x[j]=1)\text{Pr}(x[j]=1)\\&\quad\times\log_2\frac{\text{Pr}(y[j+N]=0|x[j]=1)}{\sum_{x[j]\in\{0,1\}}\text{Pr}(y[j+N]=0|x[j])\text{Pr}(x[j])}\\&\quad+\text{Pr}(y[j+N]=1|x[j]=0)\text{Pr}(x[j]=0)\\&\quad\times\log_2\frac{\text{Pr}(y[j+N]=1|x[j]=0)}{\sum_{x[j]\in\{0,1\}}\text{Pr}(y[j+N]=1|x[j])\text{Pr}(x[j])}\\&\quad+\text{Pr}(y[j+N]=1|x[j]=1)\text{Pr}(x[j]=1)\\&\quad\times\log_2\frac{\text{Pr}(y[j+N]=1|x[j]=1)}{\sum_{x[j]\in\{0,1\}}\text{Pr}(y[j+N]=1|x[j])\text{Pr}(x[j])}, \quad (55)\end{aligned}$$

where $\text{Pr}(x[j]=1)=\beta$, $\text{Pr}(x[j]=0)=1-\beta$, and $\text{Pr}(y[j+N]\in\{0,1\}|x[j]\in\{0,1\})$ can be expressed in terms of $(P_D^d[j+N])$ and $(P_F^d[j+N])$ as

$$\begin{aligned}&\text{Pr}(y[j+N]=0|x[j]=0)=1-P_F^d[j+N],\\&\text{Pr}(y[j+N]=1|x[j]=0)=P_F^d[j+N],\\&\text{Pr}(y[j+N]=0|x[j]=1)=1-P_D^d[j+N],\\&\text{Pr}(y[j+N]=1|x[j]=1)=P_D^d[j+N].\end{aligned}$$

The channel achievable rate $C[k]$ of the CN-assisted diffusive channel with mobile nanomachines, as k approaches ∞ [43], is now obtained by maximizing the mutual information $I(X[j],Y[j+N])$ over the slots $1\leq j\leq k$ with respect to the input distribution parameter β as

$$C[k]=\max_{\beta}\frac{1}{(k+N)}\sum_{j=1}^{k}I(X[j],Y[j+N])\ \text{ bits/slot}. \quad (56)$$

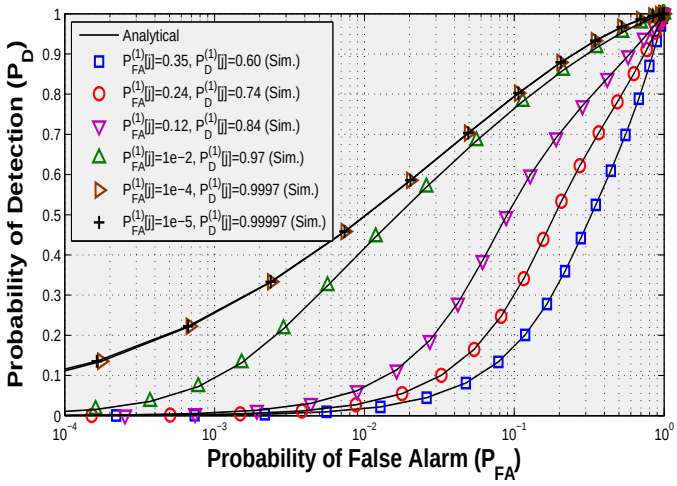

(a)

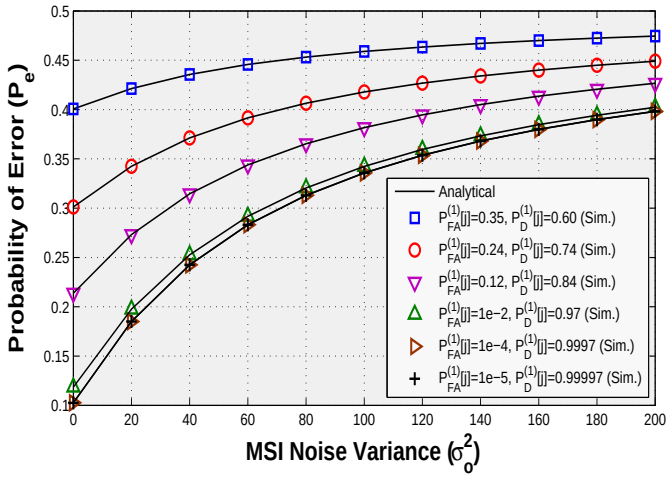

(b)

Fig. 2. Multiple CN-assisted diffusive mobile molecular system with $N = 2$ CNs where (a) demonstrates the detection performance at the DN with $\mu_o = \sigma_o^2 = 10$ and (b) demonstrates the error rate performance at the DN versus MSI noise variance σ_o^2 with $\mu_o = 10$.

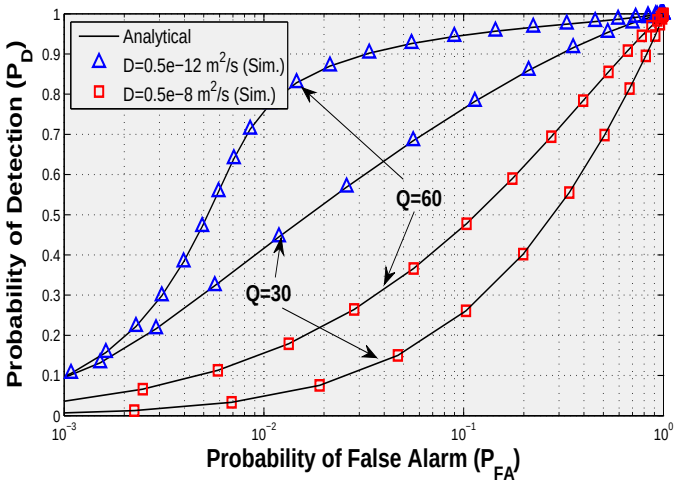

(a)

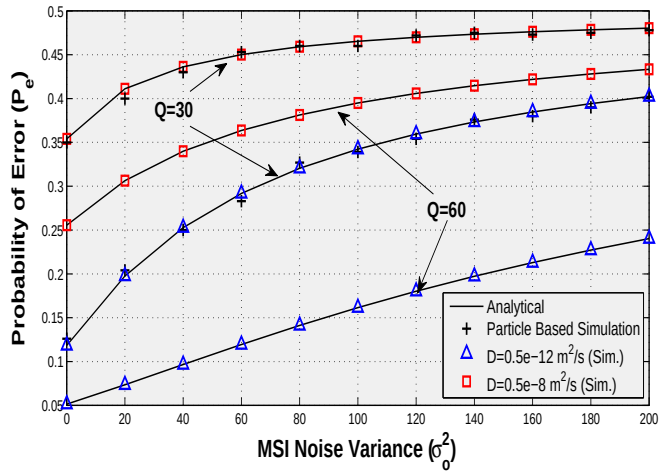

(b)

Fig. 3. Multiple CN-assisted diffusive mobile molecular system with $N = 2$ CNs, where (a) demonstrates the detection performance at the DN with $\mu_o = \sigma_o^2 = 10$ and (b) demonstrates the error rate performance at the DN versus MSI noise variance (σ_o^2) with $\mu_o = 10$.

The factor $\frac{1}{k+N}$ arises in the above expression due to the fact that $k+N$ time-slots are required to communicate k bits from the SN to the DN in the multiple CN-assisted system.

VII. Simulation Results

This section presents simulation results to demonstrate the impact of intermediate CNs on the end-to-end performance of the multiple CN-assisted diffusive mobile molecular system under various mobility conditions. For simulation purposes, the various parameters are set as mentioned in Table I unless otherwise stated. The results are computed for a total of $k = 10$ slots using Monte-Carlo simulations considering 10^5 iterations with $\mathcal{Q}_0[j] = \mathcal{Q}_0$ for $x[j] = 1$, $\mathcal{Q}_n[j+n] = \mathcal{Q}_n$ for $\widehat{x}[j+n-1] = 1, n = 1, 2$ and the diffusion coefficients, i.e., $D_{p,sn} = D_{p,rn,k} = D_p, \forall k$ are the same for different types of molecules emitted by SN and CNs. Here, we would like to emphasize that the above assumption is just to gain important insights into the system performance. However, the analysis presented in the paper considers different diffusion coefficients for different types of molecules. Further, the MSI at each receiving nanomachine is modeled as a Gaussian random variable with mean μ_o and variance σ_o^2. The counting error is also modeled as a Gaussian distributed random variable with zero mean and variance $\sigma_c^2[j]$ that depends on the average number of molecules received at the nanomachine.

Fig. 2 demonstrates the performance at the DN considering different detection performances at R_1, where R_1, R_2, and the DN are considered at initial distances 1μm, 2μm, and 3μm, respectively, from the SN at time instant $t = 0$. For simulations, the received symbols corresponding to the transmission by the mobile SN are decoded at R_1 with the probabilities of detection $P_D^{(1)}[j]$ and false alarm $P_{FA}^{(1)}[j]$ mentioned in Figs. 2a and 2b. Further, the CNs R_1, R_2, and the DN are assumed to be mobile with $D_{rn,1} = 10^{-10}$ m^2/s, $D_{rn,2} = 0.5 \times 10^{-12}$ m^2/s, $D_{dn} = 0.5 \times 10^{-12}$ m^2/s, respectively, with $v_{rn,1} = v_{rn,2} = v_{dn} = v = 10^{-3}$ m/s. Fig. 2a plots the probability of detection (P_D) versus probability of false alarm (P_{FA}) for a range of thresholds from 1 to

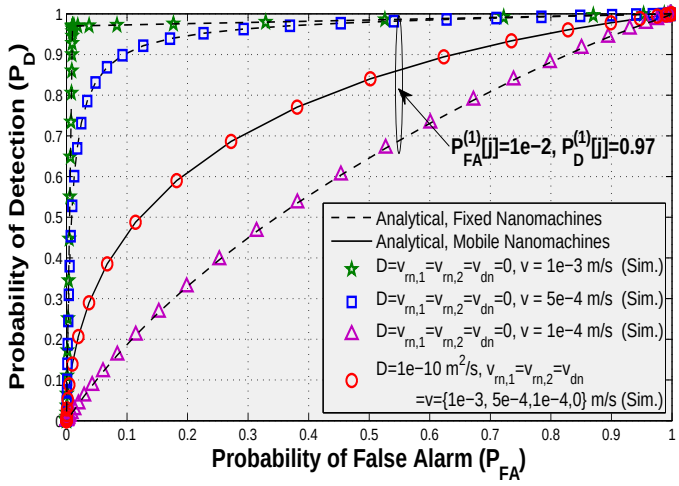

Fig. 4. Detection performance of the multiple CN-assisted diffusive molecular system considering both fixed and mobile scenarios with $\mathcal{Q}_1 = \mathcal{Q}_2 = 60$ molecules at the CNs.

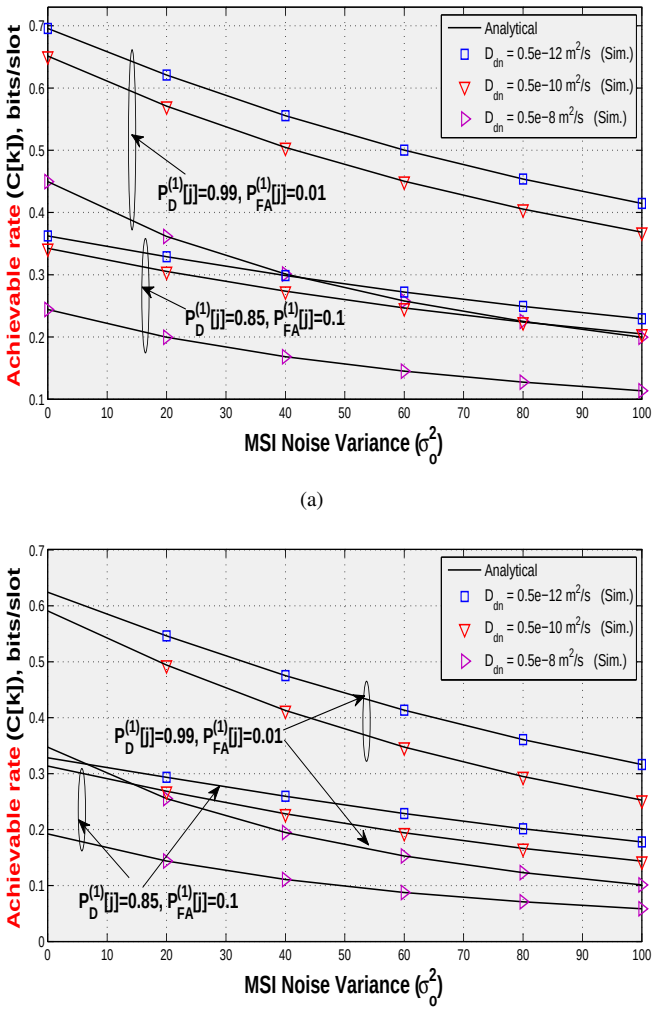

(a)

(b)

Fig. 5. Achievable rate versus MSI variance (σ_o^2) considering the presence of (a) $N = 1$ CN, where R_1 and the DN are considered at initial distances 1μm and 2μm, respectively, from the SN at $\tau = 0$ with $\mathcal{Q}_1 = 60$, $D_{rn,1}$=10^{-10} m^2/s, $v_{rn,1} = v_{dn} = v = 10^{-3}$ m/s and $\mu_o = 10$ (b) $N = 2$ CNs, where R_1, R_2 and the DN are considered at initial distances 1μm, 2μm and 3μm, respectively, from the SN at $\tau = 0$ with $\mathcal{Q}_1 = 60$, $D_{rn,1}$=10^{-10} m^2/s $D_{rn,1}$=0.5×10^{-12} m^2/s, $v_{rn,1} = v_{rn,2} = v_{dn} = v = 10^{-3}$ m/s and $\mu_o = 10$.

100 whereas Fig. 2b shows the error rate performance versus MSI noise variance (σ_o^2) with optimal thresholds derived in Section III. First, it can be observed from Figs. 2a and 2b that the analytical values derived in (31) and (47) coincide with those obtained from simulations, thus validating the analytical results. Further, both the detection and error performances at the DN significantly improve with the improvement in performance of the intermediate CN R_1. However, the performance at the DN saturates on further improvement in performance of R_1. This is due to the fact that the end-to-end performance of the multiple CN-assisted system is dominated by the weak $R_1 - R_2$ and R_2-DN links, which severely suffer from both ISI and MSI. It can also be observed in Fig. 2b that an increase in σ_o^2 results in a higher probability of error at the DN.

Fig. 3 shows the end-to-end performance of the system for a varying number of molecules at each CN under various mobility conditions, where $\mathcal{Q}_1 = \mathcal{Q}_2 = \mathcal{Q} \in \{30, 60\}$, $D_{rn,2} = D_{dn} = D \in \{0.5 \times 10^{-12}, 0.5 \times 10^{-8}\}$ m^2/s, and other parameters are considered as, $P_D^{(1)} = 0.97$, $P_{FA}^{(1)} = 0.01$, $D_{rn,1} = 10^{-10}$ m^2/s, and $v_{rn,1} = v_{rn,2} = v_{dn} = v = 10^{-3}$ m/s. One can observe that an increase in the number of molecules $\mathcal{Q}$ emitted by the CNs for transmission of symbol 1 results in a higher probability of detection at the DN for a fixed value of probability of false alarm and lower probability of error for a fixed value of σ_o^2. However, the performance deteriorates as the diffusion coefficient D increases due to higher mobility of the R_2 and DN. This is due to the fact that the probability of a molecule reaching the receiver nanomachine within the current slot decreases while the ISI from previous slots increases as diffusion coefficient D increases due to higher mobility.

Fig. 4 shows that the detection performance at the DN considering both fixed and mobile scenarios, where R_1, R_2, and the DN are considered at initial distances 1μm, 5μm, and 10μm, respectively, from the SN at time instant $t = 0$. It can be observed that the system with mobile nanomachines performs identically in a fluidic medium with and without drift. This is owing to the fact that the arrival probabilities in (1) are equivalent under both the scenarios. Further, one can also observe that the system with fixed nanomachines i.e., $D_{rn,1} = D_{rn,2} = D_{dn} = D = 0$ and $v_{rn,1} = v_{rn,2} = v_{dn} = v = 0$ under diffusion-advection flow channel with drift velocity $v \in \{1 \times 10^{-3}, 5 \times 10^{-4}\}$ m/s outperforms the scenario with mobile nanomachines. However, as the drift velocity (v) reduces to 1×10^{-4} m/s, the system with static nanomachines achieves low values of probability of detection in comparison to the one for the mobile scenario.

Fig. 5 shows the achievable rate performance of the CN-assisted diffusion-advection mobile MC system under various scenarios, where the maximum mutual information is achieved for equiprobable information symbols, i.e., $\beta = 0.5$. As depicted in Fig. 5, the achievable rate of MC decreases significantly as the variance (σ_o^2) of the MSI increases. Further, one can also observe that the achievable rate of the CN-

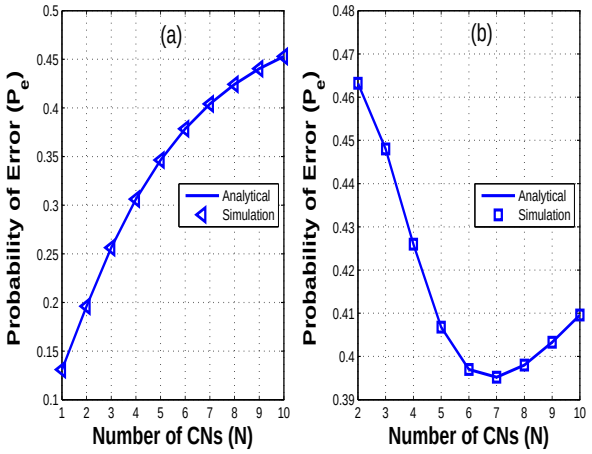

Fig. 6. Impact of number of CNs (N) or hops on the end-to-end probability of error under two different conditions: (a) the initial distance between the SN and DN is 3μm and the other parameters are considered as, $P_D^{(1)}[j] = 0.97, P_{FA}^{(1)}[j] = 0.01$, $D_p = 2.2 \times 10^{-10}$ m/s, $D_{rn,1} = 10^{-10}$ m^2/s, $D_{rn,n} = D_{dn} = 0.5 \times 10^{-10}$ m^2/s, $v_{rn,n} = v_{dn} = 1.5 \times 10^{-5}$m/s $\forall n$, $\mathcal{Q} = 100$ molecules for symbol 1, $\mu_o = \sigma_o^2 = 5$, $\tau = 30$ms, $k = 5$ slots; (b) the initial distance between the SN and DN is 30μm and the other parameters are considered as, $P_D^{(1)}[j] = 0.97, P_{FA}^{(1)}[j] = 0.01$,, $D_p = 5 \times 10^{-10}$ m/s $D_{rn,1} = 10^{-10}$ m^2/s, $D_{rn,n} = D_{dn} = 0.5 \times 10^{-8}$ m^2/s, $v_{rn,n} = v_{dn} = 10^{-3}$m/s $\forall n$, $\mathcal{Q} = 60$ molecules for symbol 1, $\mu_o = \sigma_o^2 = 5$, $\tau = 10$ms, $k = 5$ slots.

assisted system depends substantially on the detection performance of the intermediate CN R_1. As the detection performance $(P_D^{(1)}[j], P_{FA}^{(1)}[j])$ at R_1 increases from $(0.85, 0.1)$ to $(0.99, 0.01)$, a significant achievable rate gain can be achieved at low as well as high MSI for both $N = 1$ and $N = 2$ CN-based systems. However, similar to detection performance at the DN, the channel achievable rate decreases as the diffusion coefficient D_{dn} increases due to higher mobility of the DN.

Fig. 6 demonstrates the impact of number of CNs (N) on the end-to-end probability of error under two different conditions: (a) the initial distance between the SN and DN is 3μm; (b) the initial distance between the SN and DN is 30μm. It is important to note that for comparison purposes, we assumed that (i) the initial distance between the SN and DN is fixed for each of the scenarios, i.e., $N = 1, 2, \ldots, 10$ (ii) the initial distances between each of the nanomachines are equal at time instant $t = 0$, and (iii) the diffusion coefficients, i.e., $D_{p,sn} = D_{p,rn,k} = D_p, \forall k$ are the same for different types of molecules emitted by SN and CNs. From Fig. 6a, one can observe for the scenario when the initial distance between the SN and DN is not significant, the system probability of error increases as the number of CNs (N) increases. This is due to the noise accumulation in the decode-and-forward relaying protocol employed at each intermediate nanomachine. On the other hand, for the scenario when the initial distance between the SN and DN is significantly large as shown in Fig. 6b, the end-to-end performance of the system improves as N increases. Interestingly, after a certain number of CNs, i.e., $N = 7$ in our case, the performance starts deteriorating due to the retransmission of erroneously decoded symbols at each intermediate CN. Further, based on these results, one can also obtain the optimal number of CNs, i.e., 1 and 7 for the scenarios (a) and (b) respectively.

VIII. Conclusion

This work comprehensively analyzed the impact of intermediate nanomachines on the performance of multiple CN-assisted diffusive mobile MC for a diffusion-advection flow channel, considering non-idealities such as ISI, MSI, and counting errors. Closed-form analytical expressions were derived for the optimal test statistics and optimal decision thresholds at the intermediate CNs and DN, together with the resulting probability of detection, probability of false alarm as well as the end-to-end probability of error. In addition, the achievable rate of the system was also determined. Simulation results were presented to yield several interesting insights into the system performance under various mobility conditions. Finally, future research directions include the optimization of the number of transmitted molecules in each time-slot for multiple CN-assisted diffusive mobile MC.

Appendix A
Proof of Theorem 2

Let $\xi_l(n)$ denote the state of R_n with $\xi_l(n) = 1$ when R_n decodes the source information symbol as 1 and $\xi_l(n) = 0$ otherwise. Let $\xi_l = [\xi_l(1), \xi_l(2), \cdots, \xi_l(N)], 0 \leq l \leq 2^N - 1$ denote the set of 2^N binary state vectors corresponding to all the possible combinations of states of the CNs $R_1, R_2, \cdots, R_N$. For instance, the special cases of $\xi_0 = [0, 0, \cdots, 0, 0]$ and $\xi_{2^K-1} = [1, 1, \cdots, 1, 1]$ represent the state vectors corresponding to scenarios when all the CNs decode the source symbol as 0 and 1, respectively. Further, let the set Ψ_l^0 defined as $\Psi_l^0 = \{n | \xi_l(n) = 1, n = 1, 2, \cdots, N\}$, include all the CNs that decode the symbol as 1 corresponding to the overall state ξ_l given the null hypothesis $\mathcal{H}_0$. Similarly, Ψ_l^1 defines a set that includes all the CNs, which decode the symbol as 1 given the alternative hypothesis $\mathcal{H}_1$. Employing the Neyman-Pearson (NP) criterion [53], the optimal LRT $\mathcal{L}(R_{rd}[j+N])$ at the DN is given as

$$\mathcal{L}(R_{rd}[j+N]) = \frac{p(T(R_{rd}[j+N])|\mathcal{H}_1)}{p(T(R_{rd}[j+N])|\mathcal{H}_0)} \underset{\mathcal{H}_0}{\overset{\mathcal{H}_1}{\gtrless}} \frac{1-\beta}{\beta}, \quad (57)$$

where $p(T(R_{rd}[j+N])|\mathcal{H}_1)$, $p(T(R_{rd}[j+N])|\mathcal{H}_0)$ denote the likelihoods corresponding to the hypotheses $\mathcal{H}_1$ and $\mathcal{H}_0$, respectively. The test $\mathcal{L}(R_{rd}[j+N])$ above is further simplified in (58) employing the PDF $p(R_{rd}[j+N]|\xi_l)$ of the received molecules $R_{rd}[j+N]$ at the DN corresponding to the state vector ξ_l, which can be derived using the result obtained in (21) as

$$p(R_{rd}[j+N]|\xi_l) = \begin{cases} \mathcal{N}(\mu_{rd,0}[j+N], \sigma_{rd,0}^2[j+N]) \text{ if } l=0, 2, \cdots, 2^N-2 \\ \mathcal{N}(\mu_{rd,1}[j+N], \sigma_{rd,1}^2[j+N]) \text{ if } l=1, 3, \cdots, 2^N-1. \end{cases} \quad (59)$$

Further, the quantity $\Pr(\xi_l|\mathcal{H}_i), i \in \{0, 1\}$ in (58) represents the conditional probability that the network is in state ξ_l corresponding to hypothesis $\mathcal{H}_i$. Since the source and each of the CNs employ different types of molecules for transmission,

$$\mathcal{L}(R_{rd}[j+N]) = \frac{\sum_{l=0}^{2^N-1} p(R_{rd}[j+N]|\xi_l)\Pr(\xi_l|\mathcal{H}_1)}{\sum_{l=0}^{2^N-1} p(R_{rd}[j+N]|\xi_l)\Pr(\xi_l|\mathcal{H}_0)} = \frac{\sum_{l=0,2,\cdots,2^N-2} p(R_{rd}[j+N]|\xi_l)\Pr(\xi_l|\mathcal{H}_1) + \sum_{l=1,3,\cdots,2^N-1} p(R_{rd}[j+N]|\xi_l)\Pr(\xi_l|\mathcal{H}_1)}{\sum_{l=0,2,\cdots,2^N-2} p(R_{rd}[j+N]|\xi_l)\Pr(\xi_l|\mathcal{H}_0) + \sum_{l=1,3,\cdots,2^N-1} p(R_{rd}[j+N]|\xi_l)\Pr(\xi_l|\mathcal{H}_0)}, \quad (58)$$

the probability $\Pr(\xi_l|\mathcal{H}_i)$ of the system being in state ξ_l under hypothesis $\mathcal{H}_i$ follows as

$$\Pr(\xi_l|\mathcal{H}_i) = \prod_{n=1}^{N} \Pr(\xi_l(n)|\mathcal{H}_i), \quad (60)$$

where the probabilities $\Pr(\xi_l(n)|\mathcal{H}_0)$ and $\Pr(\xi_l(n)|\mathcal{H}_1)$ of the CN being in state $\xi_l(n)$ under $\mathcal{H}_0$ and $\mathcal{H}_1$, respectively, can be determined as

$$\Pr(\xi_l(n)|\mathcal{H}_0) = \begin{cases} P_{FA}^{(n)}[j+n-1], & \text{if } n \in \Psi_l^0 \\ 1 - P_{FA}^{(n)}[j+n-1], & \text{if } n \in \bar{\Psi}_l^0, \end{cases} \quad (61)$$

$$\Pr(\xi_l(n)|\mathcal{H}_1) = \begin{cases} P_{D}^{(n)}[j+n-1], & \text{if } n \in \Psi_l^1 \\ 1 - P_{D}^{(n)}[j+n-1], & \text{if } n \in \bar{\Psi}_l^1. \end{cases} \quad (62)$$

The sets $\bar{\Psi}_l^0$ and $\bar{\Psi}_l^1$ above comprise of all the CNs that decode the symbol as 0 corresponding to the network state ξ_l given hypotheses $\mathcal{H}_0$ and $\mathcal{H}_1$, respectively. The quantities $P_D^{(n)}[j+n-1]$ and $P_{FA}^{(n)}[j+n-1]$ are the probabilities of detection and false alarm, respectively, of R_n. Employing the expressions derived in (60) above, the probabilities of the system being in the state ξ_l under the hypotheses $\mathcal{H}_0$ and $\mathcal{H}_1$ can be obtained as

$$\Pr(\xi_l|\mathcal{H}_0) = \prod_{n\in\Psi_l^0} P_{FA}^{(n)}[j+n-1] \prod_{n\in\bar{\Psi}_l^0} \left(1 - P_{FA}^{(n)}[j+n-1]\right), \quad (63)$$

$$\Pr(\xi_l|\mathcal{H}_1) = \prod_{n\in\Psi_l^1} P_{D}^{(n)}[j+n-1] \prod_{n\in\bar{\Psi}_l^1} \left(1 - P_{D}^{(n)}[j+n-1]\right). \quad (64)$$

Further, substituting the Gaussian PDFs for $p(R_{rd}[j+N]|\xi_l)$ determined in (59), in the test in (58), the resulting expression can be further simplified to the form shown in (65), where the quantity β_{rd} is defined as

$$\beta_{rd} = \frac{\sum_{l=0,2,\cdots,2^N-2} [(1-\beta)\Pr(\xi_l|\mathcal{H}_0) - \beta\Pr(\xi_l|\mathcal{H}_1)]}{\sum_{l=1,3,\cdots,2^N-1} [\beta\Pr(\xi_l|\mathcal{H}_1) - (1-\beta)\Pr(\xi_l|\mathcal{H}_0)]} = \frac{(1-\beta)(1-P_{FA}^{(N)}[j+N-1]) - \beta(1-P_D^{(N)}[j+N-1])}{\beta P_D^{(N)}[j+N-1] - (1-\beta)P_{FA}^{(N)}[j+N-1]}. \quad (66)$$

The detailed derivations for the test in (65) and β_{rd} above are given in Appendix B. The expression for $f(R_{rd}[j+N])$ in (65) can be further simplified as shown in (67) by rearranging the terms. Substituting this resulting expression for $f(R_{rd}[j+N])$ in (65) followed by merging the terms independent of the received molecules $R_{rd}[j+N]$ with the threshold term in the right hand side of the equation yields the simplified test

$$(R_{rd}[j+N] + \alpha_{rd}[j+N])^2 \underset{\mathcal{H}_0}{\overset{\mathcal{H}_1}{\gtrless}} \gamma_{rd}[j+N], \quad (68)$$

where $\alpha_{rd}[j+N]$ and $\gamma_{rd}[j+N]$ are as defined in (28) and (29), respectively. Finally, since $\gamma_{rd}[j+N] \geq 0$ and $\alpha_{rd}[j+N] \geq 0$, the above expression can be simplified by taking the square root of both sides to yield the optimal test in (26).

Appendix B
Derivation of Expression (65)

Substituting the expressions given below for $p(R_{rd}[j+N]|\xi_l)$ and $p(R_{rd}[j+N]|\xi_l)$ in (58)

$$p(R_{rd}[j+N]|\xi_l) = \begin{cases} \frac{1}{\sqrt{2\pi\sigma_{rd,1}^2[j+N]}} \times \exp\left(-\frac{(R_{rd}[j+N]-\mu_{rd,1}[j+N])^2}{2\sigma_{rd,1}^2[j+N]}\right), l=1,\cdots,2^N-1 \\ \frac{1}{\sqrt{2\pi\sigma_{rd,0}^2[j+N]}} \times \exp\left(-\frac{(R_{rd}[j+N]-\mu_{rd,0}[j+N])^2}{2\sigma_{rd,0}^2[j+N]}\right), l=0,\cdots,2^N-2, \end{cases} \quad (69)$$

and cross multiplying with the threshold $\frac{1-\beta}{\beta}$, the resulting expression can be simplified as shown in (70)-(72). Subsequently, taking the logarithm of both sides of (72), the resulting expression can be further simplified to yield the expression given in (65), where β_{rd} is defined as

$$\beta_{rd} = \left[\frac{\sum_{l=0,2,\cdots,2^N-2} [(1-\beta)\Pr(\xi_l|\mathcal{H}_0) - \beta\Pr(\xi_l|\mathcal{H}_1)]}{\sum_{l=1,3,\cdots,2^N-1} [\beta\Pr(\xi_l|\mathcal{H}_1) - (1-\beta)\Pr(\xi_l|\mathcal{H}_0)]}\right]. \quad (73)$$

The probabilities $\Pr(\xi_l|\mathcal{H}_0)$, $\Pr(\xi_l|\mathcal{H}_1)$, corresponding to the system being in state ξ_l under $\mathcal{H}_0$ and $\mathcal{H}_1$, respectively, are determined as

$$\Pr(\xi_l|\mathcal{H}_0) = \prod_{n\in\Psi_l^0} P_{FA}^{(n)}[j+n-1] \prod_{n\in\bar{\Psi}_l^0} \left(1 - P_{FA}^{(n)}[j+n-1]\right),$$

$$\Pr(\xi_l|\mathcal{H}_1) = \prod_{n\in\Psi_l^1} P_{D}^{(n)}[j+n-1] \prod_{n\in\bar{\Psi}_l^1} \left(1 - P_{D}^{(n)}[j+n-1]\right).$$

Substituting the above expressions for $\Pr(\xi_l|\mathcal{H}_i)$ in (73), the expression for β_{rd} can be further simplified for different values of N as follows. To illustrate this with an example for $N=2$ CNs, the expression for β_{rd} can be evaluated considering the four possible states, i.e., $\xi_0 = [0,0], \xi_1 = [0,1], \xi_2 = [1,0]$ and $\xi_3 = [1,1]$ as $\beta_{rd} = \frac{N_2}{D_2}$, where N_2 and D_2 are given in (74) and (75) respectively. The expressions in (74) and (75) can be further simplified to yield the final expression for β_{rd} as

$$\beta_{rd} = \frac{(1-\beta)\left(1 - P_{FA}^{(2)}[j+1]\right) - \beta\left(1 - P_D^{(2)}[j+1]\right)}{\beta P_D^{(2)}[j+1] - (1-\beta)P_{FA}^{(2)}[j+1]}. \quad (76)$$

$$\overbrace{(R_{rd}[j+N]-\mu_{rd,0}[j+N])^2\sigma^2_{rd,1}[j+N]-(R_{rd}[j+N]-\mu_{rd,1}[j+N])^2\sigma^2_{rd,0}[j+N]}^{\triangleq f(R_{rd}[j+N])} \underset{\mathcal{H}_0}{\overset{\mathcal{H}_1}{\gtrless}} 2\sigma^2_{rd,0}[j+N]\sigma^2_{rd,1}[j+N]\ln\left[\sqrt{\frac{\sigma^2_{rd,1}[j+N]}{\sigma^2_{rd,0}[j+N]}}\beta_{rd}\right]. \tag{65}$$

$$\begin{aligned} f(R_{rd}[j+N]) &= R^2_{rd}[j+N](\sigma^2_{rd,1}[j+N]-\sigma^2_{rd,0}[j+N]) + 2R_{rd}[j+N](\mu_{rd,1}[j+N]\sigma^2_{rd,0}[j+N]-\mu_{rd,0}[j+N]\sigma^2_{rd,1}[j+N]) \\ &\quad + (\mu^2_{rd,0}[j+N]\sigma^2_{rd,1}[j+N]-\mu^2_{rd,1}[j+N]\sigma^2_{rd,0}[j+N]) \\ &= (\sigma^2_{rd,1}[j+N]-\sigma^2_{rd,0}[j+N])\left[R_{rd}[j+N]+\frac{\mu_{rd,1}[j+N]\sigma^2_{rd,0}[j+N]-\mu_{rd,0}[j+N]\sigma^2_{rd,1}[j+N]}{\sigma^2_{rd,1}[j+N]-\sigma^2_{rd,0}[j+N]}\right]^2 \\ &\quad - \frac{(\mu_{rd,1}[j+N]\sigma^2_{rd,0}[j+N]-\mu_{rd,0}[j+N]\sigma^2_{rd,1}[j+N])^2}{\sigma^2_{rd,1}[j+N]-\sigma^2_{rd,0}[j+N]} + (\mu_{rd,1}[j+N]\sigma^2_{rd,0}[j+N]-\mu_{rd,0}[j+N]\sigma^2_{rd,1}[j+N]). \end{aligned} \tag{67}$$

$$\begin{aligned} &\beta\left[\sum_{l=0,2,\cdots,2^N-2}\frac{\Pr(\xi_l|\mathcal{H}_1)}{\sqrt{2\sigma^2_{rd,1}[j+N]}}\exp\left(-\frac{(R_{rd}[j+N]-\mu_{rd,1}[j+N])^2}{2\sigma^2_{rd,1}[j+N]}\right)\right. \\ &\quad\left.+\sum_{l=1,3,\cdots,2^N-1}\frac{\Pr(\xi_l|\mathcal{H}_1)}{\sqrt{2\sigma^2_{rd,0}[j+N]}}\exp\left(-\frac{(R_{rd}[j+N]-\mu_{rd,0}[j+N])^2}{2\sigma^2_{rd,0}[j+N]}\right)\right] \\ &\underset{\mathcal{H}_0}{\overset{\mathcal{H}_1}{\gtrless}}(1-\beta)\left[\sum_{l=0,2,\cdots,2^N-2}\frac{\Pr(\xi_l|\mathcal{H}_0)}{\sqrt{2\sigma^2_{rd,1}[j+N]}}\exp\left(-\frac{(R_{rd}[j+N]-\mu_{rd,1}[j+N])^2}{2\sigma^2_{rd,1}[j+N]}\right)\right. \\ &\quad\left.+\sum_{l=1,3,\cdots,2^N-1}\frac{\Pr(\xi_l|\mathcal{H}_0)}{\sqrt{2\sigma^2_{rd,0}[j+N]}}\exp\left(-\frac{(R_{rd}[j+N]-\mu_{rd,0}[j+N])^2}{2\sigma^2_{rd,0}[j+N]}\right)\right], \end{aligned} \tag{70}$$

$$\begin{aligned} &\frac{1}{\sqrt{\sigma^2_{rd,1}[j+N]}}\exp\left(-\frac{(R_{rd}[j+N]-\mu_{rd,1}[j+N])^2}{2\sigma^2_{rd,1}[j+N]}\right)\sum_{l=1,3,\cdots,2^N-1}[\beta\Pr(\xi_l|\mathcal{H}_1)-(1-\beta)\Pr(\xi_l|\mathcal{H}_0)] \\ &\underset{\mathcal{H}_0}{\overset{\mathcal{H}_1}{\gtrless}}\frac{1}{\sqrt{\sigma^2_{rd,0}[j+N]}}\exp\left(-\frac{(R_{rd}[j+N]-\mu_{rd,0}[j+N])^2}{2\sigma^2_{rd,0}[j+N]}\right)\sum_{l=0,2,\cdots,2^N-2}[(1-\beta)\Pr(\xi_l|\mathcal{H}_0)-\beta\Pr(\xi_l|\mathcal{H}_1)], \end{aligned} \tag{71}$$

For $N = 3$, the expression for β_{rd} considering the eight possible states can be obtained as $\beta_{rd} = \frac{N_3}{D_3}$, where N_3 and D_3 are given in (77) and (78), respectively, which can be further simplified to yield the final expression for β_{rd} as

$$\beta_{rd} = \frac{(1-\beta)\left(1-P^{(3)}_{FA}[j+2]\right)-\beta\left(1-P^{(3)}_{D}[j+2]\right)}{\beta P^{(3)}_{D}[j+2]-(1-\beta)P^{(3)}_{FA}[j+2]}. \tag{79}$$

On the similar lines, the expression for β_{rd} considering the 2^N possible states due to the presence of N CNs can be similarly obtained as

$$\beta_{rd} = \frac{(1-\beta)\left(1-P^{(N)}_{FA}[j+N-1]\right)-\beta\left(1-P^{(N)}_{D}[j+N-1]\right)}{\beta P^{(N)}_{D}[j+N-1]-(1-\beta)P^{(N)}_{FA}[j+N-1]}. \tag{80}$$

REFERENCES

[1] N. Varshney, A. Patel, W. Haselmayr, A. K. Jagannatham, P. K. Varshney, and W. Guo, "Impact of cooperation in flow-induced diffusive mobile molecular communication," in *Proc. ASILOMAR*, 2018, pp. 1–5.

[2] T. Nakano, A. W. Eckford, and T. Haraguchi, *Molecular Communication*. Cambridge University Press, 2013.

[3] B. Atakan, *Molecular Communications and Nanonetworks*. Springer, 2016.

[4] R. Huculeci, E. Cilia, A. Lyczek, L. Buts, K. Houben, M. A. Seeliger, and T. Lenaerts, "Dynamically coupled residues within the SH2 domain of FYN are key to unlocking its activity," *Structure*, vol. 24, pp. 1947 – 1959, 2016.

[5] Y. Liu, J. Li, T. Tschirhart, J. L. Terrell, E. Kim, C.-Y. Tsao, D. L. Kelly, W. E. Bentley, and G. F. Payne, "Connecting biology to electronics: Molecular communication via redox modality," *Advanced Healthcare Materials*, vol. 6, no. 24, pp. 1 700 789 – 1 700 807, 2017.

[6] N. Farsad, D. Pan, and A. J. Goldsmith, "A novel experimental platform for in-vessel multi-chemical molecular communications," in *Proc. IEEE GlobeCom*, Dec. 2017, pp. 1 – 6.

[7] A. Llopis-Lorente, P. Diez, A. Sanchez, M. D. Marcos, F. Sancenon, P. Martinez-Ruiz, R. Villalonga, and R. Martìnez-Manez, "Interactive models of communication at the nanoscale using nanoparticles that talk to one another," *Nature Commun.*, pp. 1–7, 2017.

[8] S. Hiyama, Y. Moritani, T. Suda, R. Egashira, A. Enomoto, M. Moore, and T. Nakano, "Molecular communication," *J. Institute Electron Inf. Commun. Engineers*, vol. 89, no. 2, pp. 162–165, 2006.

[9] Y. Moritani, S. Hiyama, and T. Suda, "Molecular communication for health care applications," in *Proc. IEEE PerCom Workshops*, 2006, pp. 1–5.

$$\exp\left(\frac{(R_{rd}[j+N]-\mu_{rd,0}[j+N])^2}{2\sigma^2_{rd,0}[j+N]}-\frac{(R_{rd}[j+N]-\mu_{rd,1}[j+N])^2}{2\sigma^2_{rd,1}[j+N]}\right)\underset{\mathcal{H}_0}{\overset{\mathcal{H}_1}{\gtrless}}\sqrt{\frac{\sigma^2_{rd,1}[j+N]}{\sigma^2_{rd,0}[j+N]}}\beta_{rd}, \tag{72}$$

$$\begin{aligned}N_2=&(1-\beta)\left(1-P^{(1)}_{FA}[j]\right)\left(1-P^{(2)}_{FA}[j+1]\right)-\beta\left(1-P^{(1)}_{D}[j]\right)\left(1-P^{(2)}_{D}[j+1]\right)\\&+(1-\beta)P^{(1)}_{FA}[j]\left(1-P^{(2)}_{FA}[j+1]\right)-\beta P^{(1)}_{D}[j]\left(1-P^{(2)}_{D}[j+1]\right),\end{aligned} \tag{74}$$

$$D_2=\beta\left(1-P^{(1)}_{D}[j]\right)P^{(2)}_{D}[j+1]-\left(1-\beta)(1-P^{(1)}_{FA}[j]\right)P^{(2)}_{FA}[j+1]+\beta P^{(1)}_{D}[j]P^{(2)}_{D}[j+1]-(1-\beta)P^{(1)}_{FA}[j]P^{(2)}_{FA}[j+1]. \tag{75}$$

$$\begin{aligned}N_3=&(1-\beta)\left(1-P^{(1)}_{FA}[j]\right)\left(1-P^{(2)}_{FA}[j+1]\right)\left(1-P^{(3)}_{FA}[j+2]\right)-\beta\left(1-P^{(1)}_{D}[j]\right)\left(1-P^{(2)}_{D}[j+1]\right)\left(1-P^{(3)}_{D}[j+2]\right)\\&+(1-\beta)\left(1-P^{(1)}_{FA}[j]\right)P^{(2)}_{FA}[j+1]\left(1-P^{(3)}_{FA}[j+2]\right)-\beta\left(1-P^{(1)}_{D}[j]\right)P^{(2)}_{D}[j+1]\left(1-P^{(3)}_{D}[j+2]\right)\\&+(1-\beta)P^{(1)}_{FA}[j]\left(1-P^{(2)}_{FA}[j+1]\right)\left(1-P^{(3)}_{FA}[j+2]\right)-\beta P^{(1)}_{D}[j]\left(1-P^{(2)}_{D}[j+1]\right)\left(1-P^{(3)}_{D}[j+2]\right)\\&+(1-\beta)P^{(1)}_{FA}[j]P^{(2)}_{FA}[j+1]\left(1-P^{(3)}_{FA}[j+2]\right)-\beta P^{(1)}_{D}[j]P^{(2)}_{D}[j+1]\left(1-P^{(3)}_{D}[j+2]\right),\end{aligned} \tag{77}$$

[10] T. Nakano, M. J. Moore, Y. Okaie, A. Enomoto, and T. Suda, "Cooperative drug delivery through molecular communication among biological nanomachines," in *Proc. IEEE ICC*, 2013, pp. 809–812.

[11] B.-B. C. Youan, "Chronopharmaceutical drug delivery systems: Hurdles, hype or hope?" *Advanced drug delivery reviews*, vol. 62, no. 9-10, pp. 898–903, 2010.

[12] R. A. Freitas, "What is nanomedicine?" *Nanomed. Nanotechnol. Biol. Med.*, vol. 51, no. 6, pp. 325–341, 2005.

[13] I. Llatser, A. Cabellos-Aparicio, M. Pierobon, and E. Alarcón, "Detection techniques for diffusion-based molecular communication," *IEEE J. Sel. Areas Commun.*, vol. 31, no. 12, pp. 726–734, 2013.

[14] K. R. Liu, *Cooperative Communications and Networking*. Cambridge University Press, 2009.

[15] A. Singhal, R. K. Mallik, and B. Lall, "Performance analysis of amplitude modulation schemes for diffusion-based molecular communication," *IEEE Trans. Wireless Commun.*, vol. 14, no. 10, pp. 5681–5691, 2015.

[16] A. Einolghozati, M. Sardari, and F. Fekri, "Relaying in diffusion-based molecular communication," in *Proc. IEEE ISIT*, 2013, pp. 1844–1848.

[17] ——, "Decode and forward relaying in diffusion-based molecular communication between two populations of biological agents," in *Proc. IEEE ICC*, 2014, pp. 3975–3980.

[18] A. Ahmadzadeh, A. Noel, and R. Schober, "Analysis and design of two-hop diffusion-based molecular communication networks," in *Proc. IEEE GLOBECOM*, 2014, pp. 2820–2825.

[19] A. Ahmadzadeh, A. Noel, A. Burkovski, and R. Schober, "Amplify-and-forward relaying in two-hop diffusion-based molecular communication networks," in *Proc. IEEE GLOBECOM*, 2015, pp. 1–7.

[20] W. Guo, Y. Deng, H. B. Yilmaz, N. Farsad, M. Elkashlan, A. Eckford, A. Nallanathan, and C.-B. Chae, "SMIET: Simultaneous molecular information and energy transfer," *IEEE Wireless Commun.*, vol. 25, no. 1, pp. 106–113, 2018.

[21] Y. Deng, W. Guo, A. Noel, A. Nallanathan, and M. Elkashlan, "Enabling energy efficient molecular communication via molecule energy transfer," *IEEE Commun. Lett.*, vol. 21, no. 2, pp. 254–257, 2017.

[22] S. K. Tiwari and P. K. Upadhyay, "Estimate-and-forward relaying in diffusion-based molecular communication networks: Performance evaluation and threshold optimization," *IEEE Trans. Mol. Biol. Multi-Scale Commun.*, 2018.

[23] N. Tavakkoli, P. Azmi, and N. Mokari, "Performance evaluation and optimal detection of relay-assisted diffusion-based molecular communication with drift," *IEEE Trans. Nanobiosci.*, vol. 16, no. 1, pp. 34–42, 2017.

[24] X. Wang, M. D. Higgins, and M. S. Leeson, "Relay analysis in molecular communications with time-dependent concentration," *IEEE Commun. Lett.*, vol. 19, no. 11, pp. 1977–1980, 2015.

[25] T. Nakano and J. Shuai, "Repeater design and modeling for molecular communication networks," in *Proc. IEEE INFOCOM Workshops*, 2011, pp. 501–506.

[26] A. Ahmadzadeh, A. Noel, and R. Schober, "Analysis and design of multi-hop diffusion-based molecular communication networks," *IEEE Trans. Mol. Biol. Multi-Scale Commun.*, vol. 1, no. 2, pp. 144–157, 2015.

[27] A. Einolghozati, M. Sardari, A. Beirami, and F. Fekri, "Data gathering in networks of bacteria colonies: Collective sensing and relaying using molecular communication," in *Proc. IEEE INFOCOM Workshops*, 2012, pp. 256–261.

[28] S. Balasubramaniam *et al.*, "Multi-hop conjugation based bacteria nanonetworks," *IEEE Trans. Nanobiosci.*, vol. 12, no. 1, pp. 47–59, 2013.

[29] F. Walsh and S. Balasubramaniam, "Reliability and delay analysis of multihop virus-based nanonetworks," *IEEE Trans. Nanotechnol.*, vol. 12, no. 5, pp. 674–684, 2013.

[30] X. Wang, "1d modeling of blood flow in networks: numerical computing and applications," Ph.D. dissertation, Université Pierre et Marie Curie-Paris VI, 2014.

[31] L. Formaggia, D. Lamponi, and A. Quarteroni, "One-dimensional models for blood flow in arteries," *J. Eng. Mathematics*, vol. 47, no. 3-4, pp. 251–276, 2003.

[32] N.-R. Kim, A. W. Eckford, and C.-B. Chae, "Symbol interval optimization for molecular communication with drift," *IEEE Trans. Nanobiosci.*, vol. 13, no. 3, pp. 223–229, 2014.

[33] P. Manocha, G. Chandwani, and S. Das, "Dielectrophoretic relay assisted molecular communication for in-sequence molecule delivery," *IEEE Trans. Nanobiosci.*, vol. 15, no. 7, pp. 781–791, 2016.

[34] P.-J. Shih, C.-H. Lee, P.-C. Yeh, and K.-C. Chen, "Channel codes for reliability enhancement in molecular communication," *IEEE J. Sel. Areas Commun.*, vol. 31, no. 12, pp. 857–867, 2013.

[35] Y.-K. Lin, W.-A. Lin, C.-H. Lee, and P.-C. Yeh, "Asynchronous threshold-based detection for quantity-type-modulated molecular communication systems," *IEEE Trans. Mol. Biol. Multi-Scale Commun.*, vol. 1, no. 1, pp. 37–49, 2015.

[36] Y. Murin, N. Farsad, M. Chowdhury, and A. Goldsmith, "Time-slotted transmission over molecular timing channels," *Nano Commun. Netw.*, vol. 12, pp. 12–24, 2017.

[37] K. Srinivas, A. W. Eckford, and R. S. Adve, "Molecular communication in fluid media: The additive inverse Gaussian noise channel," *IEEE Trans. Inf. Theory*, vol. 58, no. 7, pp. 4678–4692, 2012.

[38] A. O. Bicen and I. F. Akyildiz, "System-theoretic analysis and least-squares design of microfluidic channels for flow-induced molecular communication," *IEEE Trans. Signal Process.*, vol. 61, no. 20, pp. 5000–5013, 2013.

[39] P. Rana, K. R. Pilkiewicz, M. L. Mayo, and P. Ghosh, "Benchmarking the communication fidelity of biomolecular signaling cascades featuring pseudo-one-dimensional transport," *AIP Advances*, vol. 8, no. 5, p. 055220, 2018.

[40] W. Haselmayr, S. M. H. Aejaz, A. T. Asyhari, A. Springer, and W. Guo, "Transposition errors in diffusion-based mobile molecular communication," *IEEE Commun. Lett.*, 2017.

$$
\begin{aligned}
D_3 =&\beta\left(1-P_D^{(1)}[j]\right)\left(1-P_D^{(2)}[j+1]\right)P_D^{(3)}[j+2]-(1-\beta)\left(1-P_{FA}^{(1)}[j]\right)\left(1-P_{FA}^{(2)}[j+1]\right)P_{FA}^{(3)}[j+2]\\
&+\beta\left(1-P_D^{(1)}[j]\right)P_D^{(2)}[j+1]P_D^{(3)}[j+2]-(1-\beta)\left(1-P_{FA}^{(1)}[j]\right)P_{FA}^{(2)}[j+1]P_{FA}^{(3)}[j+2]\\
&+\beta P_D^{(1)}[j]\left(1-P_D^{(2)}[j+1]\right)P_D^{(3)}[j+2]-(1-\beta)P_{FA}^{(1)}[j]\left(1-P_{FA}^{(2)}[j+1]\right)P_{FA}^{(3)}[j+2]\\
&+\beta P_D^{(1)}[j]P_D^{(2)}[j+1]P_D^{(3)}[j+2]-(1-\beta)P_{FA}^{(1)}[j]P_{FA}^{(2)}[j+1]P_{FA}^{(3)}[j+2]. \qquad (78)
\end{aligned}
$$

[41] N. Varshney, A. K. Jagannatham, and P. K. Varshney, "On diffusive molecular communication with mobile nanomachines," in *Proc. CISS*. IEEE, 2018.

[42] N. Varshney, W. Haselmayr, and W. Guo, "On flow-induced diffusive mobile molecular communication: First hitting time and performance analysis," *submitted to IEEE Trans. Mol. Biol. Multi-Scale Commun.*, 2018.

[43] T. Nakano, Y. Okaie, and J.-Q. Liu, "Channel model and capacity analysis of molecular communication with Brownian motion," *IEEE Commun. Lett.*, vol. 16, no. 6, pp. 797–800, 2012.

[44] A. Ahmadzadeh, V. Jamali, A. Noel, and R. Schober, "Diffusive mobile molecular communications over time-variant channels," *IEEE Commun. Lett.*, 2017.

[45] A. Ahmadzadeh, V. Jamali, and R. Schober, "Stochastic channel modeling for diffusive mobile molecular communication systems," *IEEE Trans. Commun.*, 2018.

[46] L. Lin, C. Yang, M. Ma, and S. Ma, "Diffusion-based clock synchronization for molecular communication under inverse gaussian distribution," *IEEE Sensors J.*, vol. 15, no. 9, pp. 4866–4874, 2015.

[47] Z. Luo, L. Lin, and M. Ma, "Offset estimation for clock synchronization in mobile molecular communication system," in *Proc. IEEE WCNC*, 2016, pp. 1–6.

[48] A. Jeffrey and D. Zwillinger, *Table of integrals, series, and products*. Academic Press, 2007.

[49] H. B. Yilmaz, C.-B. Chae, B. Tepekule, and A. E. Pusane, "Arrival modeling and error analysis for molecular communication via diffusion with drift," in *Proc. NanoCom*, 2015, pp. 86–95.

[50] L.-S. Meng, P.-C. Yeh, K.-C. Chen, and I. F. Akyildiz, "MIMO communications based on molecular diffusion," in *Proc. IEEE GLOBECOM*, 2012, pp. 5380–5385.

[51] M. Pierobon and I. F. Akyildiz, "Diffusion-based noise analysis for molecular communication in nanonetworks," *IEEE Trans. Signal Process.*, vol. 59, no. 6, pp. 2532–2547, 2011.

[52] M. H. Kabir, S. R. Islam, and K. S. Kwak, "D-MoSK modulation in molecular communications," *IEEE Trans. Nanobiosci.*, vol. 14, no. 6, pp. 680–683, 2015.

[53] S. M. Kay, "Fundamentals of Statistical Signal Processing: Detection Theory, vol. 2," 1998.

[54] B. Fagrell, M. Intaglietta, and J. Östergren, "Relative hematocrit in human skin capillaries and its relation to capillary blood flow velocity," *Microvascular research*, vol. 20, no. 3, pp. 327–335, 1980.

[55] K. Kellam and P. Altmeyer, "Capillary blood cell velocity in human skin capillaries located perpendicularly to the skin surface: measured by a new laser doppler anemometer," *Microvascular research*, vol. 52, pp. 188–192, 1996.